An active biodegradable layer-by-layer film based on chitosan-alginate-TiO_2 for the enhanced shelf life of tomatoes

Kalpani Y. Perera[a,b], Shubham Sharma[a,b,c], Brendan Duffy[c], Amit K. Jaiswal[a,b] and Swarna Jaiswal[a,b*]

[a]School of Food Science and Environmental Health, College of Sciences and Health, Technological University Dublin-City Campus, Central Quad, Grangegorman, Dublin D07 ADY7, Ireland.

[b]Environmental Sustainability and Health Institute (ESHI), Technological University Dublin-City Campus, Grangegorman, Dublin D07 H6K8, Ireland.

[c]Centre for Research in Engineering and Surface Technology (CREST), FOCAS Institute, Technological University Dublin - City Campus, Kevin Street, Dublin D08 NF82, Ireland.

*Corresponding author: Dr. Swarna Jaiswal

Email Id: swarna.jaiswal@tudublin.ie; swarna.jaiswla@outlook.com

Abstract

This work aims at developing biodegradable active chitosan-alginate layer-by-layer bio-nanocomposite film with TiO_2NPs using the solvent casting method followed by $CaCl_2$ crosslinking for food packaging applications. The developed films enhanced the tensile strength and elongation at break by 14.76 and 2 folds ($p < 0.05$) respectively. The UV barrier properties of CH-SA-0.3%TiO_2 film increased by 88.6%, while the film transparency decreased by 87.23%. All films showed antimicrobial activity against foodborne pathogens *E. coli*, *S. aureus*, *S. typhi*, and *L. monocytogene*. The film with 0.1%TiO2 showed the complete killing of gram-positive bacteria. The CH-SA-0.1%TiO_2 film was completely biodegraded during the 3 months. The CH-SA-0.3%TiO_2 film showed an increase in the shelf-life up to 8 days with stable pH, total soluble solids, and weight with no bacterial growth. Owing to their improved mechanical, UV barrier, antibacterial, and biodegradability properties the prepared films could be considered a potential candidate for fresh produce packaging.

Keywords: Chitosan; sodium alginate; TiO_2NPs; layer-by-layer; active packaging; biodegradable

1. Introduction

The increased environmental pollution has led to finding sustainable solutions for non-renewable plastic-based food packaging materials. The European Union market aims to eliminate all plastic food packaging and replace it with recyclable food packaging by 2030 (Anaya-Esparza et al., 2020). Thus, the use of biomaterial-based packaging material has become an immense trend (Anaya-Esparza et al., 2020; Kaewklin , Siripatrawan & Suwanagul, 2018; Siripatrawan & Kaewklin, 2018). The use of biodegradable bio-nanocomposites in food packaging doesn't only enables an environmentally friendly alternative but also provides a packaging system with improved properties resulting in its increased demand (Anaya-Esparza et al., 2020; Cao et al., 2020; Lan et al., 2018).

Food packaging is an essential component of food preservation since it maintains food during transportation and storage. It conserves the nutritional quality of food by protecting it from external microbial and environmental influences (de Menezes, de Lima Leita & dos Santos 2021; Yu et al., 2020). Among various food packaging materials biopolymers, chitosan and sodium alginate are of great interest because they are abundant, non-toxic, eco-friendly, biodegradable, and cost-effective (de Menezes et al., 2021; Li, Zhu & Guan 2019a).

Chitosan (CH) is a natural linear polysaccharide obtained from deacteylation of chitin has β-(1-4)-linked D-glucosamine and N-acetyl-D-glucosamine with excellent film-forming properties (Homayounpour & Shariatifar, 2020). It is also biocompatible, biodegradable, and has an excellent chelating ability (Lan et al., 2018; Li et al., 2019a). However, it has reduced mechanical properties and low antimicrobial activity (Salama, Aziz & Sabaa 2018). Sodium alginate (SA) is a

natural linear polysaccharide extracted from brown seaweed with β-Dmannuronic acid and α-L-guluronic acid components. It is a water-soluble biopolymer with gelling ability, film-forming ability, moisture absorption capability, and permeability. However, sodium alginate (SA) has poor moisture and water resistance (Lan et al., 2018; Li et al., 2019a; Salama et al., 2018). SA is a water-soluble polymer; thus, crosslinking can reduce the hydrophilicity of the polymer and increase the mechanical and thermal properties. This is done using different crosslinking molecules such as $CaCl_2$, ferulic acid, etc. while controlling the crosslinking density and swelling degree to obtain a hydrogel (Li et al., 2019a).

The two biopolymers are combined to overcome the poor mechanical properties and the water-resistance of the biopolymers. On the other hand, when CH and SA are directly combined a white insoluble polymer is created due to the electrostatic interaction between $–NH^{3+}$ of CH and $–COO^{–}$ of SA. Further, this combination when left to stand for a longer period gives a highly viscous solution. The layer-by-layer (LBL) assembly and crosslinking can be used to overcome these shortcomings of the films (Li et al., 2019a). Further, functional properties like mechanical, thermal, and barrier properties, can be enhanced by crosslinking the biopolymers (Khezerlou, Tavassoli & Sani, 2021). This LBL method is created for the development of a multilayer film taking into consideration the electrostatic interactions, hydrogen-bond interactions, and hydrophobic interactions between the macromolecules and multivalent molecules of the polymers (Li et al., 2019a).

The addition of nanofillers to the biopolymers further enhances the functional properties such as UV blocking properties, mechanical properties, antimicrobial properties, etc. TiO_2 nanoparticles (NPs) are promising candidates for food packaging due to their non-toxicity, biocompatibility,

94 low cost, physical properties, and chemical stability (Cao et al., 2020). Moreover, it has enhanced
95 UV barrier properties, ethylene scavenger activity, and antimicrobial activity (Anaya-Esparza et
96 al., 2020; Kaewklin et al., 2018; Siripatrawan & Kaewklin, 2018). TiO_2 acts as an antimicrobial
97 agent which inhibit the growth of microorganisms and increase the shelf-life of the packaged
98 food product making an active packaging material (Sani, Azizi-lalabadi & Tavassoli, 2021). TiO_2 is
99 Generally Recognized as Safe (GRAS) and is approved for use in food as the colouring additive
100 E171 (Mulla, Rahman & Marcos, 2021; Siripatrawan & Kaewklin, 2018). However, the European
101 Commission (EC) has classified TiO_2 as a category 2 carcinogen due to its inhalation hazard in
102 liquid/powder form when containing more than 1% in the particle size of aerodynamic diameter
103 ≤ 10 µm (Regulation (EU) 2018/669)(Garcia, Shin & Kim 2018). Due to its many benefits including
104 reduced food waste, and environmental pollution, antimicrobial active food packaging with
105 green materials and nanoparticles has become of great interest in the current food market (Lan ,
106 Hi, Liu, 2018). SA seaweed biopolymer has become of great interest in food packaging due to its
107 above-mentioned qualities. Thus, SA is combined with other biopolymers such as starch (Şen
108 ,Uzunsoy & Basturk, 2017), gelatine (Dou ,Li & Zhang, 2018), carboxymethyl cellulose (Ruan et
109 al., 2019), etc. to overcome its advanced properties. The combination of SA and CH will give
110 additional properties such as enhanced mechanical properties and antimicrobial activity.

111 Although many studies have been currently performed with the combination of biocompatibility
112 polymers the studies combining SA and CH are very limited (Cen et al., 2021; Li et al., 2019a).
113 Further, to our knowledge, the current study is the first to develop a CH_SA LBL film with the
114 incorporation of TiO_2. Moreover, there is a limitation in the biodegradation studies (Di Filippo et
115 al., 2021; El-Hefnawy, 2020) and application studies (Kaewklin et al., 2018; Shehata et al., 2021)

116 performed on fresh produce. Therefore, the current study aims to develop a biodegradable CH-
117 SA, LBL active packaging film with $CaCl_2$ crosslinking and the incorporation of TiO_2 NPs for cherry
118 tomato packaging applications.

119 **2. Materials and methods**

120 **2.1 Materials**

121 Chitosan (high molecular weight, MW 310000-375000 Da), sodium alginate (alginic acid sodium
122 salt from brown algae), titanium oxide nanoparticles (titanium (IV) oxide, nano-powder, 21 nm
123 primary particle size (TEM), ≥99.5% trace metals basis), glycerol (≥99.5%) and calcium chloride
124 (anhydrous, granular, ≤7.0 mm, ≥93.0%), was obtained from Sigma Aldrich (Ireland). Nutrient
125 agar, maximum recovery dilutes, and tryptone soy broth (Thermo Fisher Scientific, Ireland). The
126 foodborne pathogenic bacteria *Staphylococcus aureus* (ATCC 25923), *Listeria monocytogenes*
127 (ATCC19111), *Salmonella typhi* (ATCC140285), and *Escherichia coli* (ATCC 25922) were used in
128 this study.

129 **2.2 Development of nanocomposite films**

130 The layer by layer (LBL) films were developed with the modification of the procedures of Li et al.
131 (2019a) using the solution casting method. The Sodium Alginate (SA) solution was prepared by
132 dissolving 2g of SA in 100ml of distilled water (2% w/v). 0.5% v/v glycerol was added as a
133 plasticizer to this solution. The SA solution was stirred for 2 hours at 60°C, and 900 rpm till
134 completely dissolved. The SA solution was spread on a glass plate (30 cm × 20 cm) and dried at
135 room temperature for 24 hours. When a firm adhesive surface is obtained the SA was cross-
136 linked with 1% w/v $CaCl_2$ and dried again at room temperature for 6 hours. The chitosan (CH)
137 solution was prepared by adding 1.5% w/v CH into 100ml of 1% acetic acid. Here 0.5% v/v

138 glycerol was added as a plasticizer. Finally, various concentrations of TiO_2NPs, 0.1%w/v
139 (CH_SA_0.1%TiO_2), 0.2%w/v (CH_SA_0.2%TiO_2) and 0.3% w/v (CH_SA_0.3%TiO_2) were added to
140 the solutions. The solution was homogenized for 6 hours at 60°C, at 600rpm. The CH solution
141 was then spread on top of the SA layer and dried at room temperature for 48 hours until
142 completely dried. The dried film was cast off from the glass plate. The film was conditioned at
143 50% relative humidity (RH) and 25 °C temperature for at least 48 hours. Further, analysis was
144 performed in the LBL films, and all the tests were performed in triplicates.
145

146 **2.3 Characterisation of the bio-nanocomposite films**

147 **2.3.1 Light transmittance, UV barrier property, and surface color**

148 The color values (L (lightness), a (red-green), and b (yellow-blue)) of the films were analyzed
149 using ColorQuest XE (Hunter Lab) spectrophotometer using a standard white color plate (L=
150 97.75, a = -0.42, and b = 1.83) as a background calibrator. Six readings were taken for the
151 determination of hunter color values (L, a, and b) from different locations of each film sample.
152 The total color difference (Δ E) of the film was calculated by equation (1) (Yu et al., 2020):

153 $$\Delta E = [(\Delta L)^2+(\Delta a)^2+(\Delta b)^2]^{0.5} \quad (1)$$

154 where ΔL, Δa, and Δb respectively represent the differences between values of the white color
155 plate and prepared film.

156 The UV-light barrier and transparency of the films were determined using percent transmittance
157 at 280 nm (T280) and 660 nm (T660) respectively using the UV spectrophotometer. For these
158 rectangular films (3 cm × 7 cm) were cut and mounted between two magnetic cells of the
159 spectrophotometer.

160

161 **2.3.2 Chemical structural properties**

162 Attenuated total reflectance-Fourier transform infrared (AT-FTIR) was used to assess any
163 alteration in the functional group of nanocomposite film. FTIR spectrophotometer (Thermo
164 Scientific, Ireland) was used for the measurement of the functional groups of the films, operated
165 at a resolution of 4 cm^{1}. 4 cm × 4 cm samples of the film were placed directly on the ray
166 exposing stage and the spectrum was recorded at a wavenumber of 4000–500 cm^{-1}.

167

168 **2.3.3 Surface morphological properties**

169 The surface morphological properties of the films were obtained using the Hitachi SU-70 Scanning
170 electron microscope (SEM), USA. The films were coated with a 6nm layer of gold and Palladium and a
171 small piece of sample prepared was mounted on the sample holder of SEM for observation. The images
172 were viewed under a magnification of 10K at an operating voltage of 10 kV.

173

174 **2.3.4 Thickness, and mechanical properties**

175 A digital micrometer (VWR, Ireland) was used to measure the thickness of the film samples with
176 an accuracy of 0.001 mm at 12 random locations in the area of the film samples.

177 The mechanical strength of the packaging system is essential to secure the food during the stress
178 conditions such as storage, handling, and processing of food. The Standard ASTM D 882–88
179 method was used by Instron Universal Testing (Model 5565, Instron Engineering Corporation,
180 Canton, MA, USA) to access the mechanical strength of the packaging. The nanocomposite films
181 were cut into rectangular strips of 3 cm × 15 cm. A grip length of 50 mm and a crosshead speed
182 of 50 mm/min using a 500 N load cell set in Instron Instrument were used to operate at room

183 temperature until the sample broke at a certain point. The flexibility and strength of the film
184 were determined using tensile properties such as Tensile strength (TS), elongation at break (EB),
185 and elastic modulus (EM). The TS (MPa) and EB (%) of the films were calculated using the
186 equation (2) and (3), respectively (Zhang & Rhim, 2022).

187 $$TS = \frac{F}{X*w} \qquad (2)$$

188 $$EB = \frac{L_f - L_o}{L_o} \times 100 \qquad (3)$$

189 Where, F (N) represents the force of the film sample at the break, x (mm) is the sample
190 thickness, W (mm) is the sample width, L_f is the film elongation length at the break, and L_o
191 (50mm) is the original grasping length of the film. The EM (GPa) measures the resistance of the
192 film from being elastically deformed. The stress-strain curve in the region of elastic deformation
193 defines the elastic modulus which corresponds to the stress divided by the strain of the film
194 sample.

195

196 **2.3.5 Thermal properties**

197 Thermogravimetric analysis (TGA) was carried out on a 9 mg film sample that was scanned at
198 temperatures ranging from 30 to 500 °C at a rate of 10 °C/min. The TGA curve was used to
199 determine the weight loss (%) and maximum decomposition temperature of films.

200

201 **2.3.6 Water contact angle (WCA) and Water vapour permeability**

202 Water contact angle (WCA) determines the interaction of the film surface with the liquid
203 interphase by using a dynamic contact angle analysis (FTA-200 system). It evaluates whether the
204 surface is hydrophobic or hydrophilic. Rectangular films of 3 cm × 8 cm were placed on the

stainless-steel platform having the water contact angle analyzer attached. With the help of a micro-syringe, a drop of distilled water approximately 10 µl was dropped on the film surface. The interaction of the drop on the surface of the film was observed by taking a picture with a high-speed camera and analyzing it by the image processed by a computer.

The water vapour permeability rate (WVPR) of the films was determined gravimetrically by using the method of Salama et al. (2018). 15 g of oven dried $CaCl_2$ was placed in a circular container with a diameter of 30 mm. The top of the container was covered with the tested films (n = 3). The containers with calcium chloride without covers were left as control samples. The containers were placed in a container at a temperature of 25°C and 100% relative humidity and their weight was measured at fixed intervals (12 h) for four days. The WVPR ($g.m^2.h^{-1}$) was calculated according to formulation 4 while WVP (g.m/m2.s.Pa) is calculated as equation 5.

$$\mathrm{WVPR} = \frac{\mathrm{W}}{\mathrm{A-t}} \times 100\% \qquad (4)$$

Where W is the weight gain in grams, A is the area of the film cover, and t is the time in hours.

$$WVP = \frac{L \times WVPR}{(Pi - Pa)} \qquad (5)$$

Here, Pi = The vapor pressures of saturated air at 25°C, Pa = The vapor pressures of saturated air with RH 100% at 25°C, L = The average film thickness (m).

2.3.7 Oxygen permeability

The oxygen barrier properties of compression molded specimens (5) tested using an AMETEK OX-TRAN 2/22 OTR analyser (Minneapolis, MN, USA) in accordance with ASTM D3985. The testing gas contained 99.9% dry oxygen while the carrier gas was a combination of 98% N2 and 2% H2. The samples were evaluated at 23 °C, 50% relative humidity (RH), and 754 mmHg. The

226 sample area evaluated was 50 cm2. The OTR was given as cc/ (m2.day), and the oxygen
227 permeability (OP) is given in cc.mil/(m^2 · day) (Rodriguez-Uribe et al., 2021).

228 **2.4 Antimicrobial activity of the bio-nanocomposite films**

229 The antibacterial property of the nanocomposite film was determined through the Japanese
230 Industrial Standard (JIS Z 2801:2000) method using the foodborne pathogenic bacteria *S. aureus*
231 (ATCC 25923) (Gram-positive), *L. monocytogene* (ATCC19111) (Gram-positive), *S. typhi*
232 (ATCC140285) (Gram-negative) and *E. coli* (ATCC 25922) (Gram-negative). A kinetic study was
233 performed during periods of 0, 3, 6, 9, and 24 hours using 5 × 5 cm^2 prepared bio-nanocomposite
234 films. A test inoculum was prepared by preparing an initial bacterial concentration of 10^6
235 CFU/ml. The test setup for the antimicrobial activity was performed on a petri-dish in which a
236 filter paper was placed and wetted with sterilized water. A 5.5 × 5.5cm^2 glass slide was placed on
237 swab sticks and 400µl of the test inoculum was added and covered with the LBL films. The setup
238 was incubated for the different periods at 37°C incubators, while the spread plate method was
239 performed directly for the 0 hr samples. The antimicrobial activity was determined at the
240 different periods by placing the samples in a sterilised stomacher bag, followed by adding 10 mL
241 of Maximum Recovery Diluent (MRD) and mixing in the stomacher (AGB Scientific-Lab blender
242 400) for 40–45 s. The samples for the viable cell counts were obtained from the MRD culture
243 diluted accordingly and plated on nutrient agar plates.

244

245 **2.5 Biodegradability studies**

246 The biodegradation studies of the prepared films were carried out according to the method
247 described by Di Filippo et al. (2021). The films were cut into a size of 2 × 2cm^2. The weight of

these films was measured initially. A soil burial test was performed for 3 months by burying the films 2 cm beneath the soil. The soil temperature was around 25 °C and the soil was regularly watered to maintain the moisture. The weight of the film samples and the visual appearance of the films were determined at regular time intervals of 0, 1, 2, and 3 months. The weight loss of the film was calculated according to equation 6.

$$\text{Weight loss } \% = [(Wo-Wt)/ Wo] * 100 \quad (6)$$

Where W_0 is the initial weight and W_t is the weight at time t.

2.6 Migration test on food stimulants

For the migration studies two food stimulants were utilized 95 % (v/v) Ethanol and 3% (v/v) aqueous acetic acid. 3x5cm film samples (CH_SA control film and 0.3% TiO_2 CH_SA film) were placed in 50ml stimulants and kept at 25 °C for 10 days. The films were removed from the stimulants. To determine the TiO_2 concentration in the ethanol and acetic acid was completely evaporated before microwave digestion. After the evaporation 8 mL of nitric acid was added and then transferred into microwave digestive tubes. The microwave digestion was programmed to ramp from room temperature to 145°C in 3 minutes, hold for 5 minutes, then from 145°C to 170°C in 5 minutes, hold for 10 minutes, and then from this temperature to 190°C in 2 minutes, hold for 15 minutes. The degradation was carried out at a magnetron power of 800 w. After microwave treatment, the solution was transferred to a 50 mL vial and diluted with ultra-purified water before being used for Inductively Coupled Plasma-Mass Spectrometry (Agilent 7900 ICP-MS, Agilent Technologies). The following instrumental parameters were used for the ICP-MS analysis: lens voltage (10.5 V), ICP RF power (1100 W), CeO/Ce = 0.003, Ba^{++}/Ba^{+} = 0.014, nebulizer gas flow (0.96 $Lmin^{-1}Ar$), auxiliary gas flow (1.20 $Lmin^{-1}Ar$), plasma gas flow (15 $Lmin^{-1}Ar$). The established standard solutions were in the 0.1-200ppb Titanium standard range (Enescu et al., 2020).

271 **2.7 Effect of the LBL films on the quality of cherry tomato**

272 The cherry tomatoes were purchased at a local supermarket. Tomatoes with a good appearance
273 and physical integrity were selected for this study. Fruits were randomly distributed into groups
274 to be packaged in different films (Market films, CH_SA, 0.1%TiO_2, CH_SA, 0.2% TiO_2 CH_SA, 0.3%
275 TiO_2 CH_SA). These were then rinsed and dried before being packed with the bio-nanocomposite
276 films. Two controlled films, market packaging, and CH-SA were utilised in this research. Visual
277 appearance, weight loss, colour difference, pH, total soluble solids content (TSS), and
278 antibacterial activity of tomatoes were measured before and during storage at room
279 temperature at regular intervals of 0, 2, 4, 6, 8, 10, 15 and 15 days. The visual appearance of the
280 cherry tomato was determined during the different periods. The weight loss rate (%) of cherry
281 tomatoes was calculated by measuring the weight of the fruit before storage (W_o) and at each
282 test time point (W_t) according to equation 7 below.

283 $$\text{Weight loss } \% = [(W_o - W_t)/ W_o] * 100 \quad (7)$$

284 The L*, a*, and b* values were conducted by colourimeter to determine the colour of the cherry
285 tomato.

286 The total soluble solids (TSS) content was determined using the Brix Index (Brix). 5 g of tomatoes
287 were crushed, and the refractometer (Hand-Held Refractometer, Atago Co. Ltd., Japan) was used
288 to measure a homogenized aliquot, which was then expressed in the °Brix scale. The pH was
289 measured in the same sample using a pH meter (Eutech pH 700 Meter, 240 Lennox, Ireland). The
290 total bacterial count (TBC) of the cherry tomato was determined using the spread plate method.
291 For this, a tomato sample was transferred into a stomacher bag with 10ml MRD and
292 homogenized for 2 minutes. Which was followed by a serial dilution of the aliquot and

293 inoculating on agar plates. The results were analysed by calculating log values and evaluating the
294 log reduction in relation to the 0-hour bacterial count.
295

296 **2.8 Statistical analysis**

297 For the study of significant difference by analysis of variance (ANOVA) and the multiple
298 comparisons Fischer's least significant difference (LSD) test, the STATGRAPHICS Centurion XV
299 software (Stat Point Technologies Inc. Warrenton, VA, USA) was used. All values were expressed
300 as mean ± standard deviation (SD) and 5% significance level.

301 **3 Results and discussion**

302 **3.1 Characterization of the bio-nanocomposite films**

303 **3.1.1 Light transmittance, UV barrier properties, and surface color**

304 The light transmittance, UV barrier properties, and surface color of bio-nanocomposite films are
305 depicted in table 1. The addition of the TiO_2 NPs significantly ($p < 0.05$) improved the UV barrier
306 properties of the layer by layer (LBL) films. The UV barrier properties of the CH_SA_0.3% TiO_2
307 film significantly ($p < 0.05$) increased by 88.6% when compared to the CH_SA control film. When
308 comparing all the films 0.3% TiO_2 NPs incorporated in the film had the highest barrier properties.
309 These results are in line with the studies on where the UV barrier properties of starch-TiO_2 bio-
310 nanocomposite increase with the increasing TiO_2 concentration (Wen et al., 2018). Further, in
311 the studies of Salama & Abdel Aziz (2020), the value of UV light transmittance was reduced by
312 97.52 % after the addition of 1 wt% TiO_2 with excellent UV shielding properties. UV-light
313 transmittance decreases when TiO_2 NPs in the composite film increase, which could be
314 attributed to UV-light absorption by TiO_2 NPs (Riahi , Priyadarshi & Rhim, 2021). The free radical

generation under UV radiation can deteriorate food quality by destroying antioxidants, oxidizing lipids, degrading nutrients, changing colour, and creating off-flavors thus the UV shielding properties of the packaging film are beneficial (Wen et al., 2018). Food packaging materials containing TiO_2 NPs have high UV barrier properties because they reduce UV transmittance by absorbing/ scattering UV light. This is due to the fact that TiO_2 NP with a large surface area and high refractive index can significantly increase the light's diffuse reflection (Sani et al., 2022).

The high transparency of the packaging film allows consumers to directly inspect the contents and assess the food's quality. A transparent film, on the other hand, allows light to travel through without being filtered, lowering the quality of foods that are susceptible to photochemical reactions (Zhang & Rhim, 2022). The addition of the TiO_2 NPs significantly ($p < 0.05$) decreased the transparency of the LBL films at transmittance 600nm (T_{600}). The transparency of the CH_SA_0.3%TiO_2 film significantly ($p < 0.05$) decreased by 87.23% compared to the CH_SA control film shows lowest transmittance among all tested films. These results agree with the study of de Menezes et al. (2021) where the addition of TiO_2 NPs significantly ($p < 0.05$) increases the opacity of the CH-starch films. The TiO_2 NPs included in the layer prevent visible light from passing through, resulting in reduced light transmission (Riahi et al., 2021).

The colour of food packaging film is an important factor that influences a customer's first perception of a product and improves the product's appearance (Zhang & Rhim, 2022). The measured colour variables L*(Lightness), a*(Red-Green), b*(Yellow-Blue), and colour difference (ΔE) are listed in Table 2. The lightness (L*) of the LBL films has significantly ($p < 0.05$) decreased by 5.43% with the addition of the 0.3% TiO_2 NPs. The yellowness (b*) of the films has enhanced significantly ($p < 0.05$) by 60.15% with the addition of the 0.3% TiO_2 NPs. However, the

337 yellowness of the films has significantly ($p < 0.05$) decreased by 22.17% with the increasing 0.3%
338 TiO_2 NPs concentration. As per the studies of Goudarzi Shahabi-Ghahfarrokhi, & Babaei-Ghazvini,
339 (2017), the colour parameters are shown to be significantly reliant on the type of biopolymer
340 utilized, the interaction between biopolymers in the blends, and the quantity of TiO_2. Here, the
341 whiteness of the films increased compared to the whiteness of powdered TiO_2 NPs (Goudarzi et
342 al., 2017). Further, the results of Hosseinzadeh et al. (2020) correlate with the current results
343 where colour was accessed in chitosan- 1%w/v TiO_2 NPs where the L* was 84.01, a* was -0.80,
344 and b* were 29.48*. While the incorporation of 1%w/v TiO_2 NPs significantly increased L*, a*
345 value of films, and decreased b* value. According to the studies, TiO2 NPs significantly
346 contribute to improving the whiteness of composite films (Sani et al., 2022). These results
347 suggest that the TiO_2 NPs incorporated in films provide good optical properties, and good
348 appearance, with induced UV barrier properties, especially for light-sensitive food products.

Table 1. Surface colour, Light transmittance, and UV barrier properties of bio-anocomposite films

Film	L (Lightness)	a (Red-Green)	b (Yellow-Blue)	ΔE (Colour difference)	Transmittance T(280nm) UV barrier property	Transmittance T(600nm) film transparency
CH_SA	92.86±0.11[b]	-1.65±0.05[b]	4.65±0.14[a]	5.78±0.14[a]	88.63±0.04[c]	87.98±0.01[c]
CH_SA_0.1%TiO_2	87.59±0.11[a]	-1.56±0.02[c]	20.59±0.10[b]	21.37±0.09[d]	0.08±0.00[b]	1.29±0.02[b]
CH_SA_0.2%TiO_2	87.80±0.81[a]	-2.16±0.06[a]	14.94±0.66[c]	16.34±0.05[c]	0.07±0.00[a,b]	0.73±0.00[a]
CH_SA_0.3%TiO_2	87.82±0.17[a]	-2.12±0.02[a]	11.67±0.17[d]	14.16±0.04[b]	0.03±0.01[a]	0.66±0.11[a]

Table 2. Thickness and mechanical properties of bio-anocomposite films

Film	Thickness (mm)	Tensile Strength TS (MPa)	Elongation at Break EB (%)	Elastic modulus EM (MPa)
CH_SA	0.08±0.00[a]	1.82±0.16[a]	2.05±0.64[a]	3.39±0.16[a]
CH_SA_0.1%TiO_2	0.13±0.01[b]	22.83±0.24[c]	4.44±0.09[b]	18.11±1.65[c]
CH_SA_0.2%TiO_2	0.13±0.00[b]	26.86±0.28[d]	3.66±0.63[b]	22.04±0.77[d]
CH_SA_0.3%TiO_2	0.13±0.01[b]	11.81±1.08[b]	3.34±0.55[b]	10.86±1.41[b]

*The letters (a–d) indicate groups that are significantly different ($p < 0.05$).

3.1.2 **Chemical structural properties**

The FTIR of different films and the significant bands' wavenumber is depicted in figure 1. When considering the LBL films the absorption band at 3255 cm^{-1} represents the overlap of the stretching vibration peaks of the –OH and–NH bonds at the same place. The peak at 2877 cm^{-1} represents the vibration absorbance of C-H. The absorption band at 1644 cm^{-1} is proportional to the bending of N-H (amide II). The peak at 1410 cm^{-1} corresponds to the angular vibration of –$(CH_2)_n$– in –CH_3. While the band at 1028 cm^{-1} represents the skeletal stretching of C-O. When considering the SA films, the band at 3169 cm^{-1} represents the stretching vibration of the hydroxyl group. The stretching vibrations are also observed in studies by Li et al., (2019a) and Salama et al. (2018). Whereas the band at 2928 cm^{-1} corresponds to the asymmetric stretching vibrations of the methylene groups. Here, the absorption peaks at 1593 cm^{-1} and 1401 cm^{-1} represent the stretching vibration of the carboxylate anion –COO− exhibits two characteristics, corresponding to the asymmetric and symmetric stretching vibration of the carboxylate group, respectively. While the band at 1018 cm^{-1} corresponds to the C–O stretching in the acetyl groups present on the SA backbone. When looking into the CH film, the band at 3255 cm^{-1} represents the -OH and-NH_2 stretching vibration of chitosan. While the band at 3169 cm^{-1} demonstrates the -CH and-CH_2 stretching vibration. The band at 1018 cm^{-1} represents C-O stretching. Finally, the bands at 1639 and 1549 cm^{-1} represent the amide I & II respectively (Li et al., 2019a; Salama et al., 2018). As observed by the results of the FTIR studies it can be predicted that the molecular interaction between LBL assemblies of the SA_CH together with TiO_2 is driven mainly by N-H covalent bonds.

(a)

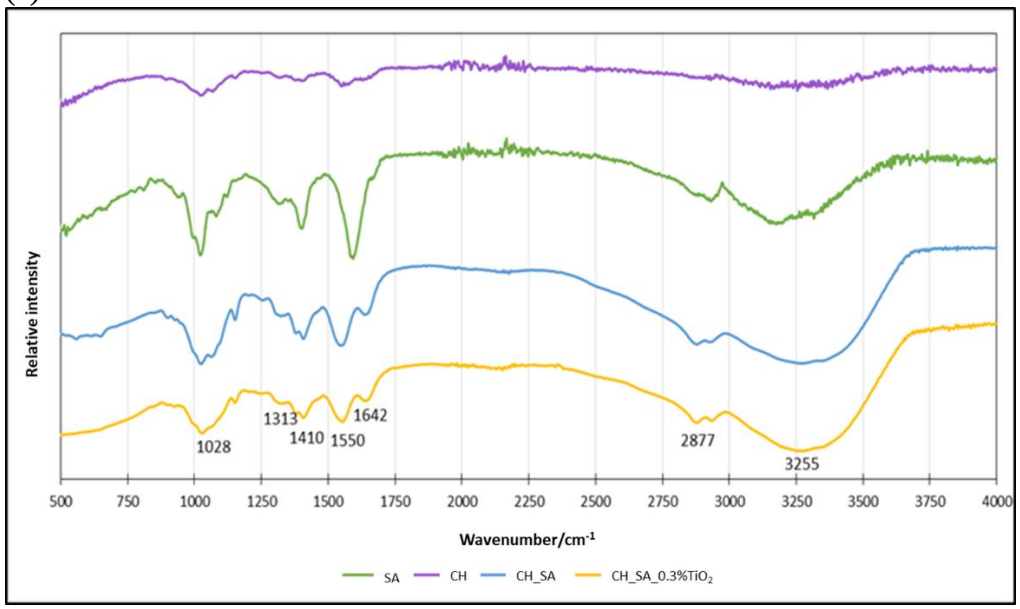

(b)

	Significant band (wavenumber/cm^{-1})			
Functional group	CH	SA	CH_SA	CH_SA_0.3 %TiO_2
C-O	1021	1021	1025	1028
O-H	-	1314	1318	1313
O-H	1402	1401	1408	1410
N-O	1550	1594	1550	1550
N-H	-	-	1631	1642
C-H	-	2929	2880	2877
O-H N-H	3255	3176	3253	3255

Figure 1. (a) AT-FTIR spectrum results of CH, SA, CH_SA, and CH_SA_0.3%TiO_2 films; (b) The significant bands of the AT-FTIR spectrum

3.1.3 Surface morphology

Figure 2(a) and 2(b) illustrates the surface morphological SEM images of CH_SA_LBL film and CH_SA_0.3%TiO_2 film respectively. Both images are shown to have a smooth surface. In addition to the smooth surface, the CH_SA_LBL film has no irregularities and is a homogenous structure. These results agree with the study of Li et al (2019a) where a smooth surface and homogenous structure were observed in the LBL SA and CH film developed by them. It suggests that the biocompatibility of CH and SA has been enhanced due to the presence of crosslinking by ferulic acid. In the current study, the $CaCl_2$ crosslinking also plays a vital role in uniformity, surface smoothness, and no irregularities. The addition of TiO_2 NPs to the CH_SA film changes the surface morphology of the films where agglomerated TiO_2 NPs are observed on the surface. These results align with the studies of Menezes et al. (2021) and Kustiningsih et al. (2019) where agglomeration, granules, and less smooth surface were observed with the addition of TiO_2 NPs. This is due to the fact that TiO_2 nanoparticles aggregate readily in mildly acidic ranges of 5 to pH 7 as a result of their neutralization of surface charges. Because 1% w/w acetic acid was used for the dissolution of CH, it should be noted that the biopolymeric blends have a mildly acidic pH. The hydrophilic -NH_2 groups from chitosan and the TiO_2 nanoparticles are hypothesized to produce intermolecular interactions (Menezes et al., 2021).

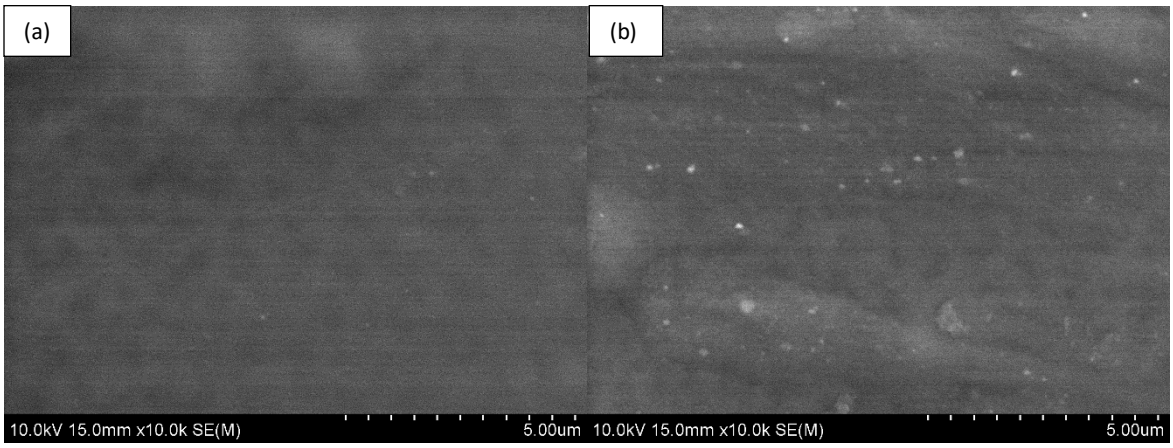

Figure 2. SEM images of (a) CH_SA_LBL film (b) CH_SA_0.3%TiO_2 film

396

397 **3.1.4 Thickness, and mechanical properties**

398 The mechanical properties of an active food packaging film are essential to prevent packaging
399 failure, encountered during storage and distribution. The internal structure of the film matrix
400 and the interaction between the filler and the film matrix determine the mechanical properties
401 of an active film (Zhang & Rhim, 2022). The thickness and the mechanical properties of the LBL
402 films are represented in table 1.

403 The thickness of all the TiO_2 NPs incorporated in films was approximately 0.13 mm. The thickness
404 of the films significantly ($p < 0.05$) increased with the addition of TiO_2 NPs. Hence, it can be
405 predicted that the thickness of the films was influenced by the type of material or substance and
406 their interaction (Li et al., 2019a).

407 The mechanical properties of films can be influenced by the type of polymer and the interaction
408 between its components (Li et al., 2019a). The tensile strength (TS) of the films increased
409 significantly ($p < 0.05$) up to 14.76 folds with the addition of TiO_2 NPs. The TS of the films has
410 reached a maximum of 0.2% TiO_2 NPs incorporated films. These results correspond to the studies
411 of Siripatrawan and Kaewklin (2018) wherewith increasing TiO_2 NPs concentration the TS
412 reached a maximum value of 16.43 MPa (by ~1.5 folds) at 1% (w/w) TiO_2 (equals to 0.02%w/v
413 TiO_2) and then decreased by ~1.5 folds (when compared to 1% w/w TiO_2)at 2% (w/w) TiO_2
414 (Siripatrawan & Kaewklin, 2018). In this study, the maximum value of TS is observed at 26.86MPa
415 (0.2% TiO_2 NPs) and decreased by 2.27 folds (0.3% TiO_2 NPs) hereafter. When compared to this
416 study the TS of the present study has further increased, which may be due to the LBL structure of
417 the film. To some extent, the LBL assembly can improve the mechanical properties with
418 enhanced molecular interaction by increasing the contact area between them (Li et al., 2019a).

419 However, different results were observed in the study of de Menezes et al. (2021) when TiO_2 NPs
420 were added to a matrix of chitosan and cassava starch, when 0.25% TiO_2 is added, TS reduces
421 significantly, but 0.5% TiO_2 causes a 15% increase in TS. This maybe is due to the different
422 biopolymer combinations and the crosslinking technique.
423 The TiO_2 NPs concentration plays an important role in particle agglomeration which affects the
424 TS of the nanocomposite films. At 0.25-1% TiO_2 NPs concentrations, the TiO_2 NPs could uniformly
425 disperse in the chitosan matrix and may perform as a reinforcing filler by strengthening the film
426 network (Siripatrawan & Kaewklin, 2018). The TS results obtained in this study can be reflected
427 in the fact that the matrix of the nanocomposite might be reinforced through electrostatic
428 interactions, hydrogen bonding, or O-Ti-O bonding by adding a considerable quantity of TiO_2 NPs
429 which can be observed by the FTIR studies (figure 1). However, an inhomogeneous distribution
430 of agglomerated TiO_2 NPs may disrupt this equilibrated nanocomposite system, resulting in
431 matrix breakage and a loss in film TS (Siripatrawan & Kaewklin, 2018).
432 The elongation at break (EB) increased by approximately 2 folds in the 0.2% TiO_2 NPs
433 incorporated in LBL films. However, the EB was slightly reduced by 1-fold with increased 0.3%
434 TiO_2 NPs concentrations. This is by the study of Cao et al. (2020) the elongation at break was first
435 increased by 2.5 folds to the maximum at 5% (w/w) of TiO_2 / Ag NPs content and then decreased
436 by 2.2 folds (10% w/w TiO_2 / Ag NPs). The reduction of elongation at break and tensile strength
437 with 10% (w/w) NPs content was due to the agglomeration of NPs acting like defects in the
438 polymer network (Cao et al., 2020). However, the study by Siripatrawan and Kaewklin (2018)
439 concluded that the EB significantly decreased by 1.2 folds when TiO_2 NPs is added to the chitosan
440 matrix with no significant difference with the TiO_2 NP concentration. The increase of the EB in

441 the current study may be due to the layer by layer nature of the structure with the SA and CH
442 matrix together with TiO_2 NPs. The EM significantly improved up to 6.5 folds with the addition of
443 TiO_2 NPs into the films. The EM of the films has reached a maximum of 22.04 MPa with 0.2% TiO_2
444 NPs incorporated in films.
445 Thus, when considering the mechanical properties CH_SA_0.2%TiO_2 LBL film had the most
446 enhanced properties when compared to all the other films. These results clearly show that
447 including TiO_2 NPs at insufficient concentrations of 0.2% w/v could result in mechanical property
448 improvements via electrostatic interactions and hydrogen bonding. The improved mechanical
449 properties of the films are attributed to the combined effects of LBL structure, TiO_2 NPs
450 concentration, $CaCl_2$ crosslinking, and glycerol plasticizer. The amounts of calcium and glycerol
451 had a synergistic effect, resulting in good strength and fracture strain properties (Wen et al.,
452 2018).
453 The thermal stability of materials used in the packaging industry is critical. The ability of a film to
454 withstand degradation at high temperatures is reflected in its thermal property.
455

456 **3.1.5 Thermal stability**

457 Thermogravimetric analysis (TGA) is widely used to determine a film's thermal stability (Zhang et
458 al., 2019). The TGA curves are displayed in figure 2. As observed by the curves there are two
459 significant stages of weight loss in all the film samples. The first stage of weight loss is the
460 evaporation of the film moisture occurred in the temperature range of 60–180 °C, with the
461 weight decreasing by about 20%. The second stage of weight loss takes place in the temperature
462 range of 210–400°C and was caused by thermal degradation of the films in each case (Li et al.,

2019a). Here there is a drastic reduction in the weight loss of the films which attributes to the depolymerization, dehydration, deamination, and cleavage of glycosidic Linkages in the films (Sun et al., 2021). All the LBL films are not completely degraded at 500 °C and ~30% of all the films were remaining at 500 °C. When TiO_2 NPs were added to control film specimens, the TGA curve of this sample resembled that of the control sample, indicating that the addition of TiO_2 NPs did not affect the film's thermal stability. The studies of Li et al. (2019b) and Liu et al. (2021) also found the TiO_2 addition didn't influence the thermal stability of the biopolymer films. However, the studies of Lan et al. (2021) contradict these results where they discovered that the TiO_2 NPs might considerably increase the thermal stability of chitosan films because of their heat resistance feature and reduced mobility of the polymer chain of films. Here also ~20% of all the films were remaining at 800 °C.

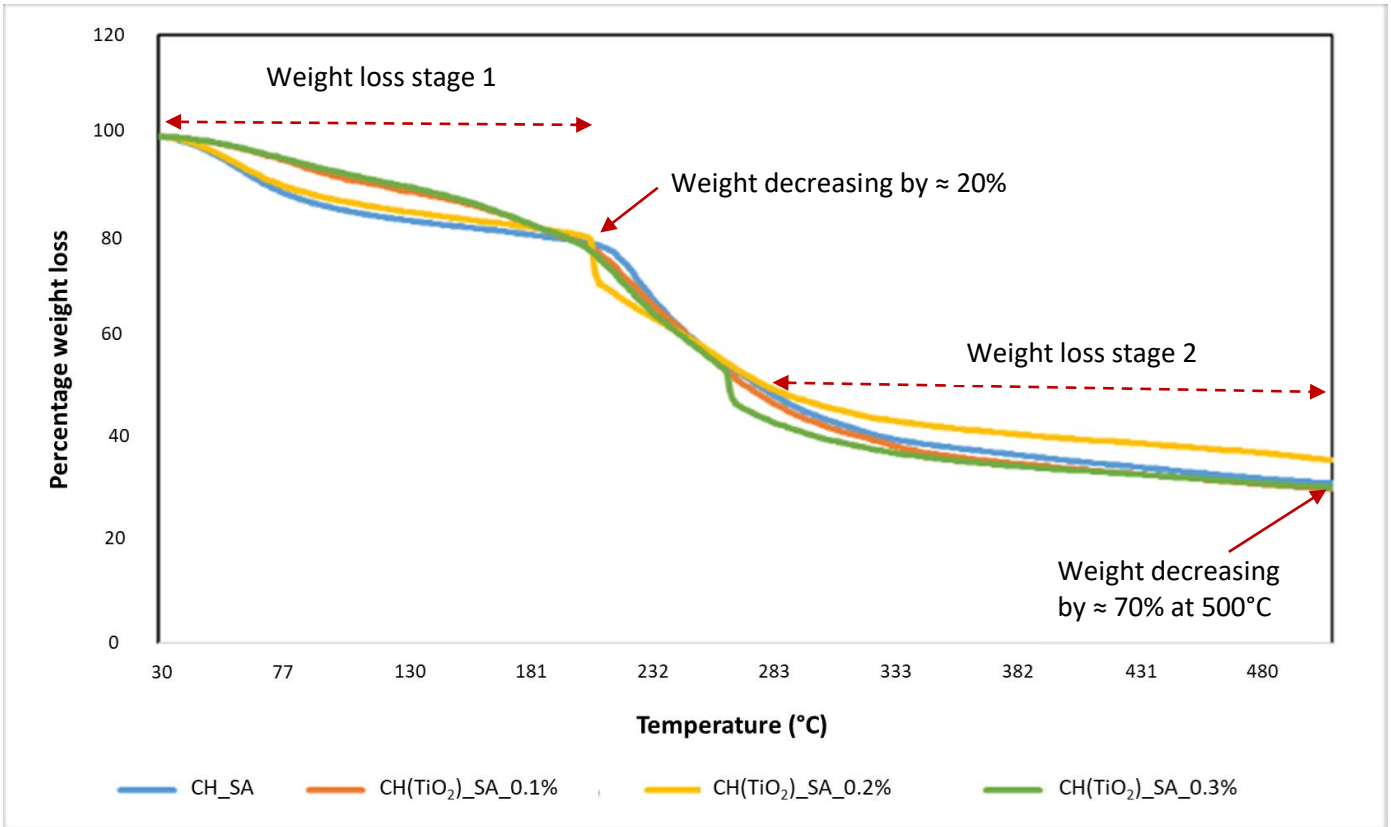

Figure 2. Thermogravimetric curves of CH_SA, CH_SA_0.1%TiO_2, CH_SA_0.2%TiO_2 and CH_SA_0.3%TiO_2 films.

3.1.6 Water contact angle (WCA) and Water vapour permeability rate (WVPR)

Enhanced water vapour barrier properties of a packaging film can extend the shelf life of foods sensitive to moisture changes (Zhang & Rhim, 2022). The WCA is a collective method to determine the hydrophobicity of the films. The WCA of all the LBL films is displayed in table 3. The WCA is higher by 0.96 folds in the control film when compared to the other films. However, the WCA of the films increased significantly ($p < 0.05$) by 1.32 folds with the increasing TiO_2 NPs. Thus, the films are more hydrophobic with the increasing TiO_2 NP concentration. These results agree with the results of Xiong , Sheng & Wang, (2019) where the WCA of starch films is increased up to 1.9 folds (10% TiO_2) with the increasing TiO_2 NP concentration. Thus, TiO_2 NPs can effectively increase the hydrophobicity of films in higher concentrations of more than 0.2% TiO_2 NPs. However, all the films in the present study are hydrophilic as the WCA is <90°. The WCA of SA and 2.5 wt.% TiO2 NPs were found to be 53° (Tang et al., 2018). While the WCA of CH-0.05 W/V% TiO_2 film was 44.4° (Zhang et al., 2017). When compared to these studies the WCA of the current study, CH_SA_0.3%TiO_2 66.44° is higher due to a combined effect of CH, SA, TiO_2, and $CaCl_2$ crosslinking. Most biopolymer-based films are hydrophilic, they can absorb moisture and degrade when used to package foods with high moisture content, this restricts their use in dried food products packaging (Zhang & Rhim, 2022).

The WVP is an important criterion for packaging films to evaluate the water transferred from the food to its environment. For a film to be suitable for dry food packing, the WVP should be as low

as possible to avoid dehydration of the food product (Salama et al., 2018). In the current study, the WVPR of the films has significantly ($p < 0.05$) increased by 3.31% when compared to the control film. Further, the water permeability rate has increased by 1-fold with the increasing TiO_2 NPs concentration from 0.1 to 0.3%. This may be due to the nature of the biopolymer which increases the WVP of the membrane. Thus, the current packaging material is not suitable for the packaging of dry food products. However, they are suitable to increase the shelf-life of fresh products such as fruits and vegetables. Furthermore, the biodegradability rate of hydrophilic films are much higher when compared to hydrophobic films due to its degradation properties in soil and water (Ahari & Soufiani, 2021). The Water vapor permeability decreased in the study of Lan et al. (2021) when TiO_2 NPs were added to the matrix. The increase in WVP in the current instance may be due to the presence of SA biopolymer.

Table 3. Water contact angle (WCA) and Water vapor permeability rate of LBL films.

Film	**Water Contact Angle (WCA)(°)**	**WVPR ($g.m^2.h^{-1}$)**
Control (without film)	-	68.28 ± 0.04^a
CH_SA	69.48 ± 2.7^c	68.54 ± 0.08^b
CH_SA_0.1%TiO_2	50.38 ± 1.39^a	69.32 ± 0.19^c
CH_SA_0.2%TiO_2	57.62 ± 2.22^b	69.32 ± 0.09^c
CH_SA_0.3%TiO_2	66.44 ± 2.18^c	70.89 ± 0.10^d

*The letters (a–d) indicate groups that are significantly different ($p < 0.05$).

512 **3.1.7 Oxygen permeability**

513 It's crucial for food packing materials to be oxygen resistant. An excessive amount of oxygen
514 dissemination from the environment into food products may result in oxidative rancidity and loss of
515 value, quality, and nutritional content (Jafarzadeh & Jafari, 2020). It may also deteriorate flavor, aroma,
516 texture, and appearance, changing the food's value, quality, and shelf life. The OP was performed on the
517 control CH_SA film and the film with the highest concentration of TiO_2 (CH_SA_0.3%TiO_2). The OTR was
518 2.31±0.09 cc/ (m^2.day) and 1.95±0.49 cc/ (m^2.day) respectively for the CH_SA and CH_SA_0.3%TiO_2 film.
519 While the OP was 5.92±0.87 cc.mil/(m^2.day) and 4.93±0.56 cc.mil/(m^2.day) respectively for the CH_SA
520 and CH_SA_0.3%TiO_2 film. The results show that the OP of the films decreases by 20.18% with the
521 addition of 0.3% TiO_2 NPs. By acting as a physical barrier to prevent gas from passing through the
522 nanocomposite films, the impermeable nanoparticles reduce the effective permeability. TiO_2 NPs make it
523 necessary for the permeating gas to follow a tortuous path through the polymer matrix (Zamanian et al.,
524 2021). As per the study of Zamanian et al. (2021) the combination of montmorillonite nanoclay and
525 titanium oxide TiO_2 NPs increases the barrier properties of polyvinyl alcohol films by 59%.

526 **3.2 Antimicrobial activity of the bio-nanocomposite films**

527 Antibacterial properties are critical for food packaging films as the foodborne pathogens can
528 degrade food quality, resulting in food spoilage, which can ultimately lead to various diseases
529 (Zhang et al., 2019). The antimicrobial activity of the LBL films for 0, 3, 6, 9, and 24 hours against
530 four foodborne pathogens *E. coli*, *S. aureus*, *S. typhi,* and *L. monocytogene* is displayed in figure
531 3. When compared to the control films, CH_SA_0.1%TiO_2 films showed a complete killing of
532 Gram-positive bacteria (*S. aureus* and *L. monocytogenes*) with the log reduction of 7.28 log
533 CFU/mL and 6.02 log CFU/mL respectively after 24 h of exposure. However, the complete killing
534 of Gram-negative bacteria *E. coli* and *S. typhi* with a log reduction of 7.08 log CFU/mL and 6.04

535 log CFU/mL respectively were observed on the CH_SA_0.3%TiO_2 film with the higher
536 concentration of TiO2.
537 Here, only a reduction of 2.35 log CFU/mL and 1.91 log CFU/mL were found for *E. coli* and *S.*
538 *typhi*, respectively for the CH_SA_0.1%TiO2 LBL films. Thus, it can be observed from these
539 studies that the antibacterial activity of the films is significantly ($p < 0.05$) higher for Gram-
540 positive bacteria when compared to Gram-negative bacteria. Nevertheless, enhanced
541 antibacterial properties are observed in the CH_SA_0.3%TiO_2 when considering all 4 tested
542 foodborne pathogens.
543 Similarly, the results of Shanmugam et al. (2020) indicated that the TiO_2 NPs showed higher
544 antibacterial activity against *S. aureus* when compared with *E. coli*. As per the study, TiO_2 NPs
545 chitosan-sodium alginate scaffolds showed inhibition zones of 18.56 ± 0.88 mm and 21.45 ± 0.25
546 mm against *E. coli* and *S. aureus*, respectively. Here a higher antimicrobial activity is observed
547 against Gram-positive *S. aureus* when compared to Gram-negative bacteria (*E. coli)* because of
548 the separation of cytoplasm from the bacterial cell wall or plasmolytic activity of the cell wall.
549 TiO_2 NPs can damage bacteria cells by interacting with sulfur-containing cell membrane proteins
550 and phosphorus-containing cell components like DNA, resulting in cell death. Nanoparticles
551 easily permeate the cell membrane and limit the function of respiratory enzymes, resulting in
552 the production of reactive oxygen species (ROS) and the facilitation of DNA damage. In addition,
553 the photocatalysis of TiO_2 NPs implies the disintegration of *E. coli*'s outer membrane leading to
554 increased antimicrobial activity (Shanmugam et al., 2020). The complex cell wall and extra
555 lipopolysaccharide outer membrane on Gram-negative bacteria's surface, which make it difficult
556 for TiO_2 NPs to enter the cell wall, may account for their increased resistance to TiO_2 NPs (Sani et

557 al., 2022). Further, in the studies of Zhang et al. (2019) with chitosan, TiO_2 NPs, and anthocyanin
558 the antimicrobial activity of Gram-positive bacteria was more effective than Gram-negative
559 bacteria. Where inhibitions zones of 5.83 ± 0.21mm, 6.68 ± 0.11mm, 6.74 ± 0.20mm, and
560 7.12 ± 0.14mm were observed for the CH_0.8% w/v TiO_2 NPs film for *E. coli*, *S. typhi*, *S. aureus*,
561 and *L. monocytogenes* respectively. TiO_2 NPs have a wide range of antimicrobial characteristics
562 because the antibacterial activity of NPs has increased with increasing contact time and
563 concentration of NPs against tested microorganisms. The ability of NPs to suppress or inhibit
564 microorganism's results from two main mechanisms: free metal ion toxicity caused by the
565 dissolution of metals from the surface of NPs and oxidative stress caused by the production of
566 ROS on the surface of NPs using organic hydroperoxides and hydrogen peroxide. Thus, NPs can
567 influence bacterial survival by accumulating on their surface and altering the structure of their
568 DNA, proteins, peptidoglycans, and lipids. The generation of ROS , such as hydrogen peroxide,
569 superoxide, and hydroxyl radicals, as well as artificial light, UV light intensity, shape, and size, all
570 affect the antimicrobial activity of TiO2 NPs. These active species damage the bacteria by
571 destroying its outer membrane, which contains phospholipids, proteins, and lipopolysaccharides
572 (Alizadeh-Sani et al., 2020a).

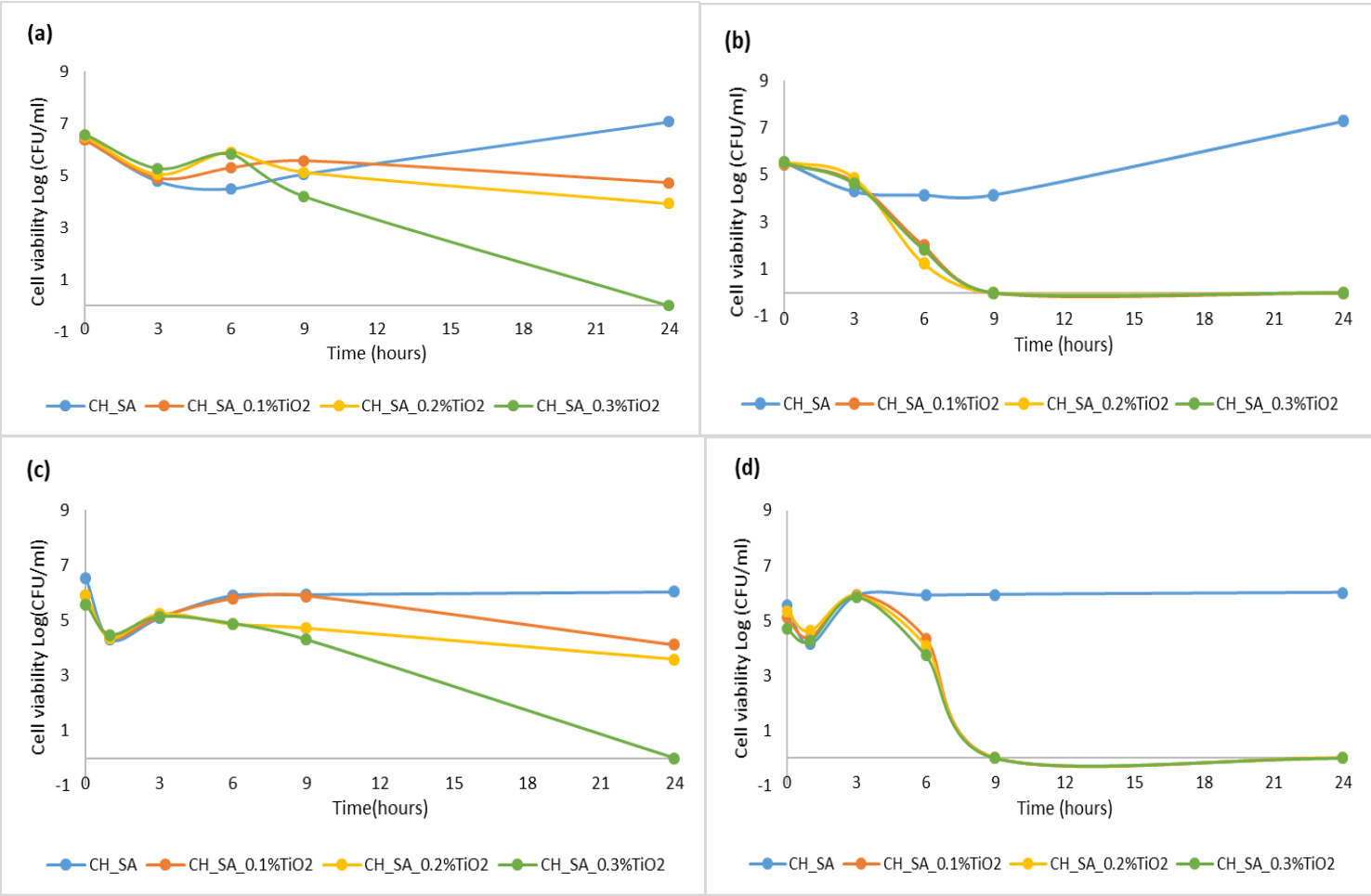

Figure 3. Antimicrobial efficiency of LBL bio-nanocomposite films. (a) efficiency of LBL on *E. coli*, (b)efficiency of LBL on *S. aureus*, (c) efficiency of LBL on *S. typhi* and (d) efficiency of CH_SA, CH_SA_0.1%TiO_2, CH_SA_0.2%TiO_2 and CH_SA_0.3%TiO_2 LBL on *L. monocytogenes*

579

580 **3.3 Biodegradability studies of the prepared bio-nanocomposite films**

581 Each biopolymer degrades in its unique fashion, depending on intrinsic parameters like
582 crystallinity, chemical structure, molecular weight, surface area, and crosslinks, as well as
583 external soil elements like temperature, moisture, pH, and microbial composition (Pires , Souza
584 & Fucinos, 2022). The biodegradation studies of the prepared films were carried out for 3
585 months. The appearance of the films during the biodegradation study can be seen in figure 4.
586 The weight loss of the LBL films during the biodegradation is presented in table 4. When
587 considering the weight loss during biodegradation the CH_SA and CH_SA_0.1%TiO_2 films were
588 completely biodegraded during the 3 months. Wherein the percentage weight loss of the
589 CH_SA_0.2%TiO_2 and CH_SA_0.3%TiO_2 films were 93.75±0.94% and 89.06±1.04% respectively.
590 Thus, from the weight loss results of the biodegradation studies, it can be observed that the
591 biodegradation is significantly ($p < 0.05$) reduced by 10.95% with the increased NP concentration
592 from 0.1%TiO_2 to 0.3%TiO_2. The results of the current study agree with that of El-Hefnawy,
593 (2020) where the increased TiO_2 NP concentration increases the biodegradation time of the
594 chitosan bio-nanocomposite films during hydrolytic degradation. The biodegradation process
595 was affected by the increased TiO_2 NPs concentration however the mass reduction is observed
596 over a prolonged period. This is because the antimicrobial properties of TiO_2 NPs delay microbial
597 degradation of films, causing the films to have a slower biodegradation rate (El-Hefnawy, 2020).
598 However, in the studies of polymers such as Polylactic acid, TiO_2 NPs have increased the rate of
599 biodegradation since the water molecules easily penetrated the nanocomposites (Luo ,Lin &
600 Guo, 2019).

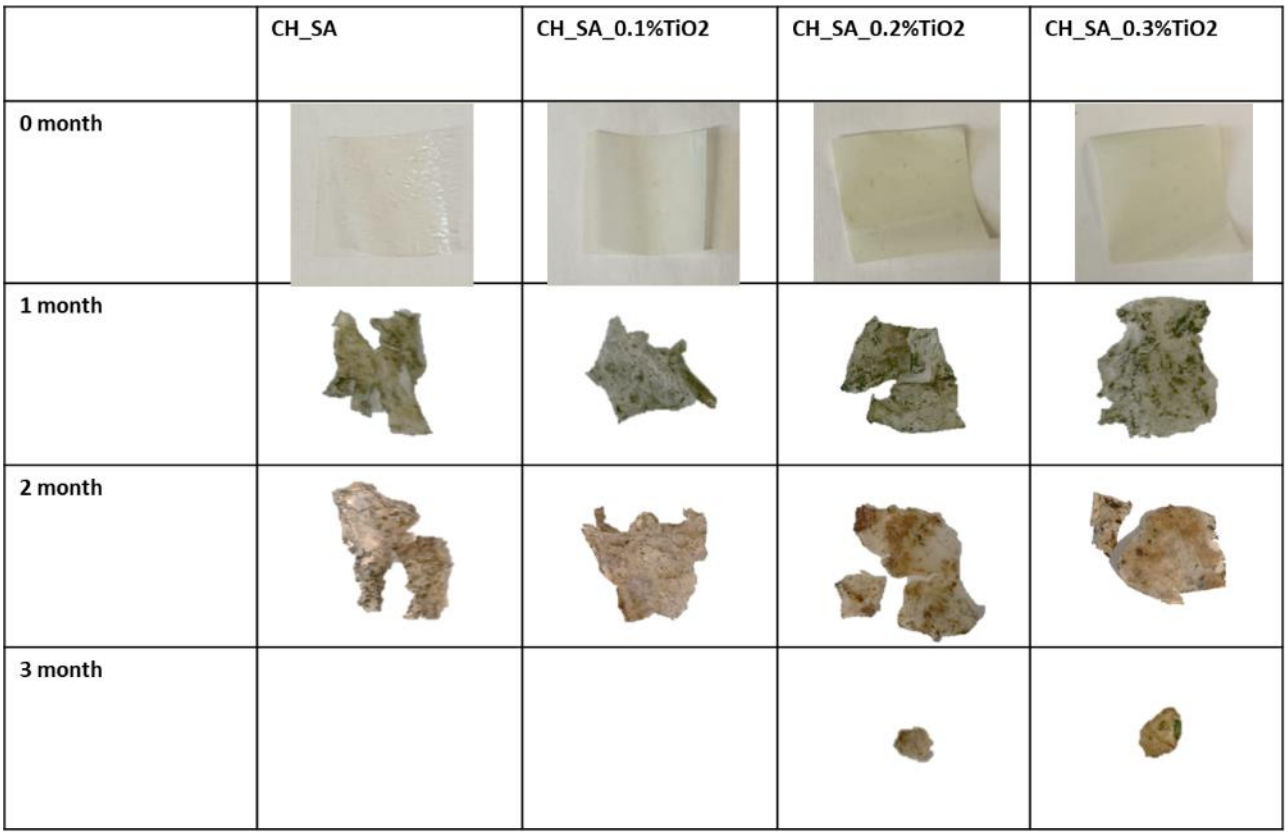

Figure 4. The appearance of the films during the biodegradation studies of the LBL films for 3 months

Table 4. Percentage weight loss during biodegradable studies.

	CH_SA	**CH_SA_0.1%TiO_2**	**CH_SA_0.2%TiO_2**	**CH_SA_0.3%TiO_2**
0 month	0±0	0±0	0±0	0±0
1 month	42.47±1.2^{b}	70.12±5.48^{b}	59.40±2.86^{b}	53.32±10.20^{a,b}
2month	70.89±5.50^{a,b}	72.15±6.33^{a,b}	70.02±3.25^{a}	79.26±0.09^{b}
3month	100±0^{c}	100±0^{c}	93.75±0.94^{b}	89.06±1.04^{a}

*The letters (a–d) indicate groups that are significantly different ($p < 0.05$).

3.4 Migration test on food stimulants

608 Chemical contamination of food due to the migration of packaging components contaminants
609 that could compromise the safety and organoleptic properties (Phothisarattana &
610 Harnkarnsujarit, 2022). Thus it is essential that there is limited or no migration of components
611 especially NPs into food products. Thus, the study on migration of the TiO_2 NPs from the LBL film
612 was performed in two food stimulants; 95% ethanol and 3% acetic acid, at 25°C for 10 days. Here
613 the study was performed in the control films and the film with the highest concentration of TiO_2
614 NPs CH_SA_0.3%TiO_2. As per the current study, a migration of 124.93±4.10 ng/L and
615 332.03±13.47 ng/L was observed respectively for 95% ethanol and 3% acetic acid, at 25°C for 10
616 days. The overall migration limits in both the food stimulants are much lower than the total
617 legislative migration limit (0.01 mg/kg food) which is set by European commission regulation (EC)
618 No. 450/2009 for non-authorized substances (European Commision, 2009). As per the study by
619 Enescu et al. (2020) the migration level of Ti of the chitosan-TiO_2 NPs film was 220.4 ± 5.9 ng/L at
620 10 days at 40°C. Furthermore, as per the study of Phothisarattana & Harnkarnsujarit (2022) on
621 thermoplastic starch, polybutylene adipate-co-terephthalate, and TiO_2 NPs, the overall migration
622 levels are 0.2-1.3 mg/dm^2, which is higher than the current study. The competitive process of
623 nanoparticle migration depends on the compatibility of nanoparticles with both liquid (food) and
624 solid (film) media during the surface swelling of the solid phase as it comes into getting close to
625 the liquid phase (Enescu et al., 2020). Thus, the lower migration rate of the nanoparticles in the
626 current study may have been related to steric obstructive effects or as a result of the
627 development of highly attractive interactions in the biopolymer matrix between the TiO_2 and
628 other elements (Alizadeh-Sani et al., 2020b).
629

630 **3.5 Effect of the LBL films on the quality of cherry tomato during storage**

631 The effect of the prepared active films on cherry tomatoes was determined for a storage period
632 of 15 days at room temperature (20-24°C) while testing was carried out at regular intervals. Here
633 two control films were used, one was the market film and the other the CH_SA film. The
634 appearance of the cherry tomato reduced during the storage period as observed in figure 5.
635 Whereas the colour changes of the tomato is highlighted in table 5. As in similar studies, wilting,
636 shriveling, colour change and degradation may cause the appearance to deteriorate during
637 storage (Shehata et al., 2021). As observed in the figure TiO_2 NPs were able to improve the
638 appearance of the tomato during storage and increased the shelf-life of the tomato up to 10
639 days with the CH_SA_0.3%TiO_2 film. These cherry tomatoes were without any putridity, with no
640 juice leaking, and visualized a glossy surface. Wherein, bacterial growth is observed in the
641 market film after 6 days. These findings support previous findings that tomatoes have a
642 climacteric ripening pattern regulated by ethylene and that ripened tomatoes can be stored at
643 7–10°C with a relative humidity of 85–90% for up to 4–7 days (Sooch & Mann, 2021).

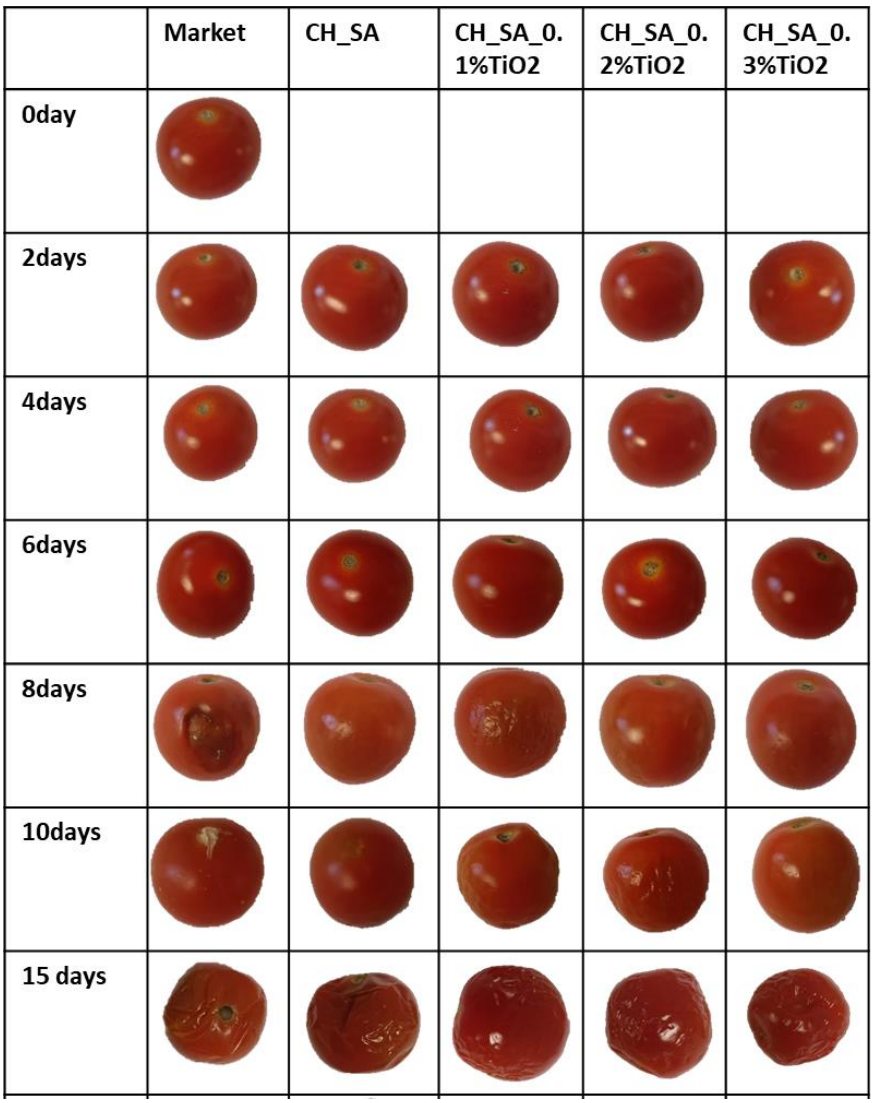

Figure 5. The appearance of cherry tomato packed in different packaging materials (CH_SA, CH_SA_0.1%TiO_2, CH_SA_0.2%TiO_2 and CH_SA_0.3%TiO_2) up to 15 days of storage at room temperature

Table 5. Colour changes of packaged cherry tomato during storage

		Market	CH_SA	CH_SA_0.1%TiO_2	CH_SA_0.2%TiO_2	CH_SA_0.3%TiO_2
0day	L*	44.78±0.36^{a}	44.78±0.36^{a}	44.78±0.36^{a}	44.78±0.36^{a}	44.78±0.36^{a}
	a*	25.78±2^{a}	25.78±2^{a}	25.78±2^{a}	25.78±2^{a}	25.78±2^{a}
	b*	29.96±0.24^{a}	29.96±0.24^{a}	29.96±0.24^{a}	29.96±0.24^{a}	29.96±0.24^{a}
2day	L*	43.73±1.22^{b}	43.76±0.36^{b}	44.29±0.90^{b}	41.46±0.17^{a}	45.59±0.68^{c}
	a*	31.97±0.91^{b}	29.48±0.50^{a}	28.81±1.22^{a}	34.59±1.43^{c}	29.02±0.28^{a}
	b*	36.81±2.71^{b}	35.62±0.67^{a,b}	36.31±0.91^{b}	33.57±0.57^{a}	33.90±0.77^{a}
4day	L*	42.72±0.55^{b}	43.29±0.37^{b,c}	41.16±0.83^{a}	41.33±0.48^{a}	43.89±0.70^{c}
	a*	29.79±0.93^{a,b}	28.45±0.99^{a}	30.49±1.17^{b,c}	29.47±0.37^{a,b}	31.41±0.69^{c}
	b*	27.37±0.8^{b}	27.41±0.46^{b}	24.92±1.29^{a}	24.60±0.73^{a}	28.44±0.75^{b}
6day	L*	41.91±0.93^{b}	40.53±0.37^{a}	41.96±0.29^{b}	40.96±0.44^{a}	40.53±0.52^{a}
	a*	31.02±0.59^{b,c}	30.39±0.42^{a,b,c}	31.55±1.66^{c}	29.84±0.41^{a,b}	29.33±0.57^{a}
	b*	25.35±0.98^{b}	23.49±0.62^{a}	26.16±0.48^{b}	23.92±0.66^{a}	22.98±0.49^{a}
8day	L*	43.48±1.55^{b,c}	44.32±1.02^{b}	41.54±0.45^{a}	43.60±0.54^{b,c}	42.49±0.52^{a,b}
	a*	31.03±3.66^{c}	29.85±0.5^{b,c}	29.03±0.17^{b,c}	25.31±2.32^{a}	26.56±2.36^{a,b}
	b*	29.41±1.63^{b}	30.64±0.64^{b}	26.26±0.75^{a}	29.34±0.8^{b}	27.41±0.63^{a}
10day	L*	45.93±0.28^{c}	41.62±0.24^{b}	41.93±0.26^{b}	39.60±0.6^{a}	46.22±0.69^{c}
	a*	30.43±4.44^{a}	30.81±0.55^{a}	31.48±0.86^{a}	30.00±0.53^{a}	27.89±0.94^{a}
	b*	30.65±2.74^{c}	25.77±0.28^{b}	26.38±0.65^{b}	22.96±0.71^{a}	33.99±1.28^{d}
15 day	L*	37.41±0.64^{a}	36.47±0.86^{a}	37.55±0.59^{a}	37.74±0.95^{a}	39.69±0.08^{b}
	a*	21.02±0.69^{a}	25.74±0.39^{b}	33.24±1.21^{d}	29.65±0.5^{c}	31.82±1.53^{c}
	b*	26.65±1.19^{a}	28.15±0.75^{b}	28.19±0.68^{b}	28.40±0.84^{a}	31.65±0.11^{d}

*The letters (a–d) indicate groups that are significantly different ($p < 0.05$).

650

651 The weight of a food product is an important parameter to determine its quality and shelf-life.
652 The weight loss of the fruits takes place due to the loss of moisture content (Othman, Othman &
653 Shapi'i, 2021). As anticipated weight loss percentage of cherry tomatoes increased with storage
654 periods. As observed in figure 6(a) the weight loss of CH_SA_0.3%TiO_2 film was significantly ($p <$
655 0.05) 1 fold low when compared to the other films.

656 Total soluble solids (TSS) evaluate fruit ripening in the fruit. TSS content in tomato fruit for all
657 films increased up to 5.07°Bx with prolongation of the storage period until the 6th day of storage
658 and then decreased up to 1.27°Bx until the end of storage as depicted in figure 6(b). When
659 compared with the tomatoes packaged in the market film the TSS levels of the tomatoes
660 packaged in CH_SA_0.3%TiO_2 films were 3.26 folds higher ($p < 0.05$) at the end of 15 days of
661 storage. TSS of tomatoes increased as they matured from pink stage to red ripen. The increase in
662 TSS content in tomato fruit during the first period of storage might be explained by the moisture
663 loss during storage. The decline in TSS content in tomato fruit after 6 days from storage might be
664 due to the consumption of total sugar in the respiration process during storage. Chitosan-
665 containing films maintained the highest level of TSS content in tomato fruit throughout the
666 storage period as compared to the control. Chitosan controls the respiration process and their
667 related metabolic activities leading to an accumulation of sugar content (Shehata et al., 2021).
668 Similar results are observed in the studies of Kaewklin et al. (2018) where there was an increase
669 in the TSS during the storage of packed tomatoes (Kaewklin et al., 2018).

670 The normal pH range for cherry tomatoes is between 4.30 and 4.9. The pH values of the tomato
671 samples packaged in the different packaging materials are depicted in figure 6(c). All the samples

packaged in all the films were within this range until the 10th day. However, the pH of the market film and the CH_SA film was significantly ($p < 0.05$) reduced after the 15 days and were not in the above-mentioned range. As per the study of Shehata et al. (2021), the pH value of the cherry tomato progressively decreases up to 3.6 with the increasing storage time of 21 days when treated with chitosan. In the study of Shahbazi , Shavisi & Karami, (2021) where strawberry was coated with okra mucilage-quince seed mucilage, cellulose nanofibers, and Eryngium planum extract. The uncoated strawberry had the highest pH of 4.47, while cellulose nanofibers, and Eryngium planum extract coated samples had the lowest pH between 3.33 to 3.62. This is contradiction result with the current study which had the lowest pH for market and control films at the end of 15 days. This maybe mainly due to the different fruits used in the study. The increase of the organic acids such as citric acid results in weight loss which results in increased pH during strawberry storage. However as per the studies of Al-Dairi, Pathare & Al-Yahyai, (2021) on tomato storage a high reduction in titratable acidity i.e. the percentage of citric acid was observed sue to the increased storage temperature and ripening. The change of the pH value of the current study maybe a result of the changed TSS and titratable acidity value.

The total bacterial count (TBC) of the packaged tomato was evaluated at regular periods as observed in figure 6(d). In all samples, the initial TBC was less than 1 log CFU/mL, indicating that the fruits' initial microbiological quality was good (Shahbazi & Shavisi, 2020). Here, the TBC of the tomato samples a bacterial growth of 2.15 log CFU/mL was observed at 6 days. While no bacterial growth was observed in all the other cherry tomatoes packaged in the other films at 6 days. When evaluating the 8th day of storage CH_SA_0.3%TiO_2 film was able to inhibit the bacterial growth while bacterial growth of 5.98 log CFU/mL and 3.13 log CFU/mL was observed

694 respectively in tomatoes packaged in the market and CH_SA control films. Thus,
695 CH_SA_0.3%TiO_2 film can increase the shelf-life of cherry tomatoes up to 8 days without any
696 bacterial growth. Similar results are observed in the studies of Sooch and Mann (2021) where
697 the TBC was lower in the TiO_2 NPs incorporated in packaging films when compared to the market
698 tomato packaging. Further, in the studies of Cao et al. (2020) Poly (butylene adipate-co-
699 terephthalate) - 5% (w/w) TiO_2- Ag packaged tomato had the lowest antimicrobial growth at 14
700 days and no antimicrobial growth at 7 days, confirming that TiO_2 NPs plays a great role in the
701 reduced microbial growth. Further, it has been confirmed by the studies of Shahbazi & Shavisi
702 (2020) and Shahbazi et al. (2021) on banana coatings and strawberry coatings respectively. The
703 TBC has increased with storage time. However, the coated fruits had lower bacteria growth
704 because it acts as a semi-permeable barrier to oxygen which reduce the food spoilage.

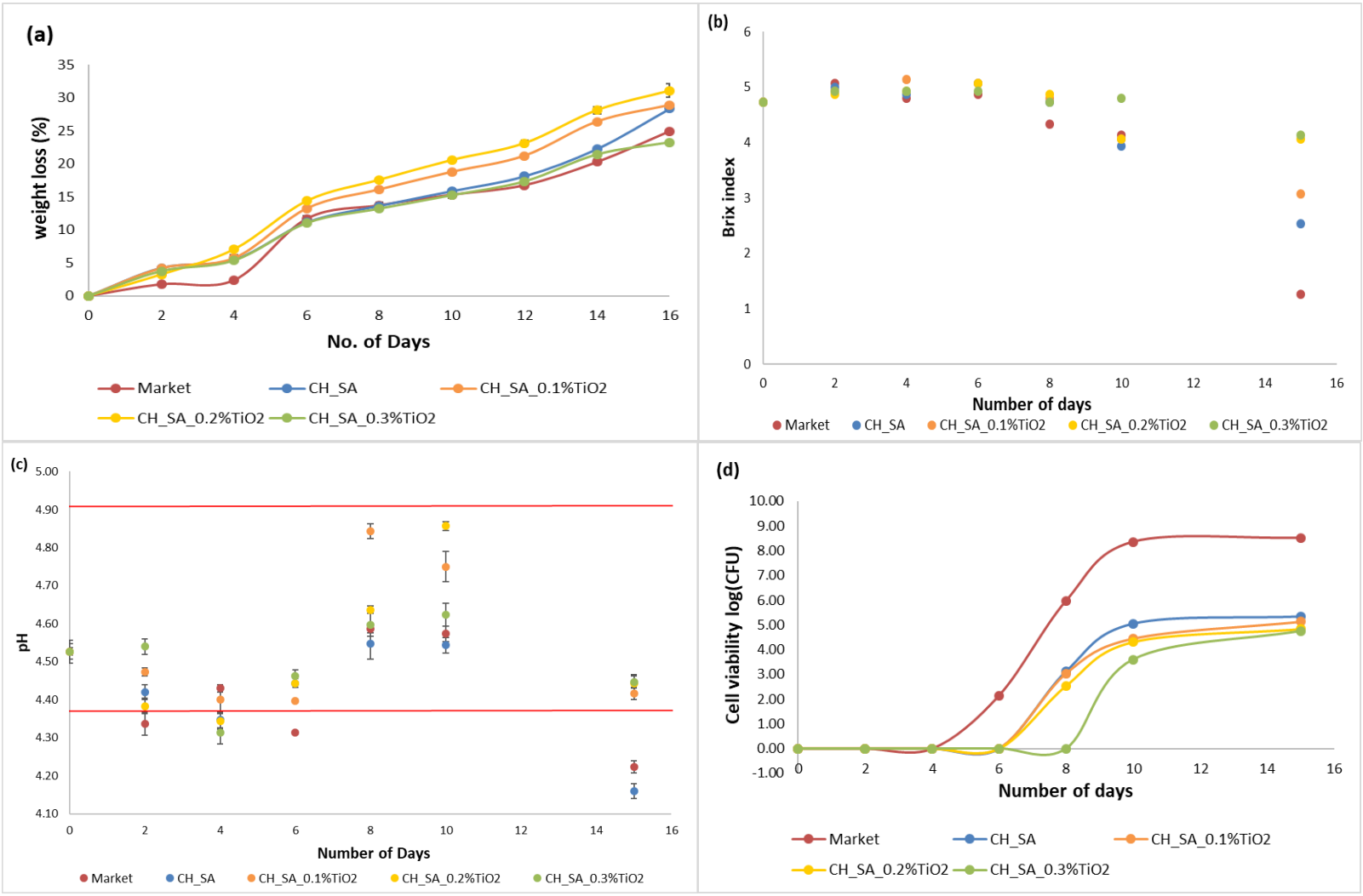

Figure 6. Shelf-life studies of tomato for a time period of 0 to 15 days (a) weight loss percentage of packaged cherry tomato, (b) total soluble solids in tomato, (c) pH change in packaged tomato, and (d) total bacteria count (TBC) of packaged tomato.

710

711 **4 Conclusion**

712 In this study biodegradable active food packaging material was developed using CH, SA, and TiO_2
713 NPs in an LBL structure with $CaCl_2$ crosslinking. The developed packaging material enhanced the
714 mechanical properties where tensile strength was significantly increased ($p < 0.05$) by 14.76 folds
715 and EM was significantly increased ($p < 0.05$) by 2 folds when 0.2% w/v TiO_2 NPs is incorporated
716 into the LBL film. The UV barrier properties significantly increased ($p < 0.05$) by 88.6% with the
717 addition of 0.3% w/v TiO_2 NPs. Further, films with lower concentration TiO_2 (0.1%) showed
718 complete killing of Gram-positive bacteria, however no growth of Gram-negative bacteria was
719 observed on the films with 0.3% TiO_2 concentration after 24 h of exposure. In addition,
720 CH_SA_0.1%TiO_2 LBL film have completely biodegraded within three months. While 89.06%
721 weight loss was observed in the CH_SA_0.3%TiO_2 films within the 3 months of soil degradation.
722 Finally, the CH_SA_0.3%TiO_2 LBL packaging material was able to prolong the shelf-life of
723 tomatoes by up to 8 days. Based on the obtained results, the prepared CH_SA_0.3%TiO_2 LBL
724 active packaging films could be considered a potential candidate for fresh produce due to their
725 improved mechanical, UV barrier, antibacterial properties, and biodegradability. Further, studies
726 should be performed on the LBL bio-nanocomposite films such as life cycle assessment, toxicity
727 analysis, migration studies, techno-economic analysis, and testing against many more fruit and
728 vegetable products to develop the packaging film in the industrial market.

729

730 **Author Contributions:** K.Y.P.: Conceptualization, Formal analysis, Data curation, Investigation,
731 Methodology, Laboratory work, Writing-original draft, Writing-review & editing. S.S.:

732 Methodology, Laboratory work. B.D.: Resources. S.J.: Methodology, Formal analysis, Validation,
733 Resources, Supervision, Writing-review & editing. A.K.J.: Funding acquisition, Project
734 administration, Conceptualization, Resources, Supervision, Writing-review & editing. All authors
735 have read and agreed to the published version of the manuscript.

736

737 **Acknowledgments:** The authors would like to acknowledge the funding from Technological
738 University Dublin under the Researcher Award- 2021.

739

740 **Conflicts of Interest:** The authors declare no conflict of interest.

741 **References**

742 1. Ahari, H., & Soufiani, S. P. (2021). Smart and Active Food Packaging: Insights in Novel
743 Food Packaging. Frontiers in Microbiology, 12(July), 1–26.
744 https://doi.org/10.3389/fmicb.2021.657233
745 2. Al-Dairi, M., Pathare, P. B., & Al-Yahyai, R. (2021). Chemical and nutritional quality
746 changes of tomato during postharvest transportation and storage. Journal of the Saudi
747 Society of Agricultural Sciences, 20(6), 401–408.
748 https://doi.org/10.1016/j.jssas.2021.05.001
749 3. Alizadeh-sani, M., Id, H. H., Khezerlou, A., Maleki, M., & Azizi-, M. (2020a). Kinetics
750 Analysis and Susceptibility Coefficient of the Pathogenic Bacteria by Titanium Dioxide and
751 Zinc Oxide Nanoparticles. 10(1), 56–64. https://doi.org/10.15171/jcvtr.2015.24
752 4. Alizadeh-Sani, M., Mohammadian, E., & McClements, D. J. (2020b). Eco-friendly active
753 packaging consisting of nanostructured biopolymer matrix reinforced with TiO2 and

754 essential oil: Application for preservation of refrigerated meat. Food Chemistry,
755 322(April), 126782. https://doi.org/10.1016/j.foodchem.2020.126782
756 5. Anaya-Esparza, L. M., Villagran-de la Mora, Z., Ruvalcaba-Gomez, J. M., Romero-Toledo,
757 R., Sandoval-Contreras, T., Aguilera-Aguirre, S., Montalvo-Gonzalez, E., & Perez-Larios, A.
758 (2020). Use of Titanium Dioxide (TiO2) Nanoparticles as Reinforcement Agent of
759 Polysaccharide-Based Materials. *Processes, 8*(11), Article 1395.
760 https://doi.org/10.3390/pr8111395
761 6. Cao, C. L., Wang, Y. Y., Zheng, S. M., Zhang, J., Li, W., Li, B. B., Guo, R. J., & Yu, J. (2020).
762 Poly (butylene adipate-co-terephthalate)/titanium dioxide/silver composite biofilms for
763 food packaging application. *Lwt-Food Science and Technology, 132*, Article 109874.
764 https://doi.org/10.1016/j.lwt.2020.109874
765 7. Cen, S., Fang, Q., Tong, L., Yang, W., Zhang, J., Lou, Q., & Huang, T. (2021). Effects of
766 chitosan-sodium alginate-nisin preservatives on the quality and spoilage microbiota of
767 Penaeus vannamei shrimp during cold storage. International Journal of Food
768 Microbiology, 349(April), 109227. https://doi.org/10.1016/j.ijfoodmicro.2021.109227
769 8. de Menezes, F. L., de Lima Leite, R. H., Gomes dos Santos, F. K., Aria, A. I., & Aroucha, E.
770 M. M. (2021). TiO2-enhanced chitosan/cassava starch biofilms for sustainable food
771 packaging. *Colloids and Surfaces A: Physicochemical and Engineering Aspects, 630*,
772 127661. https://doi.org/https://doi.org/10.1016/j.colsurfa.2021.127661
773 9. Di Filippo, M. F., Dolci, L. S., Liccardo, L., Bigi, A., Bonvicini, F., Gentilomi, G. A., Passerini,
774 N., Panzavolta, S., & Albertini, B. (2021). Cellulose derivatives-snail slime films: New

775 disposable eco-friendly materials for food packaging. *Food Hydrocolloids, 111*, Article
776 106247. https://doi.org/10.1016/j.foodhyd.2020.106247
777 10. Dou, L., Li, B., Zhang, K., Chu, X., & Hou, H. (2018). Physical properties and antioxidant
778 activity of gelatin-sodium alginate edible films with tea polyphenols. International Journal
779 of Biological Macromolecules, 118, 1377–1383.
780 https://doi.org/10.1016/j.ijbiomac.2018.06.121
781 11. El-Hefnawy, M. E. (2020). Biodegradable Films from Phytosynthesized
782 TiO(2)Nanoparticles and Nanofungal Chitosan as Probable Nanofertilizers. *International*
783 *Journal of Polymer Science, 2020*, Article 6727132.
784 https://doi.org/10.1155/2020/6727132
785 12. Enescu, D., Dehelean, A., Gonçalves, C., Cerqueira, M. A., Magdas, D. A., Fucinos, P., &
786 Pastrana, L. M. (2020). Evaluation of the specific migration according to EU standards of
787 titanium from Chitosan/Metal complexes films containing TiO2 particles into different
788 food simulants. A comparative study of the nano-sized vs micro-sized particles. Food
789 Packaging and Shelf Life, 26(March), 100579. https://doi.org/10.1016/j.fpsl.2020.100579
790 13. European Commision. (2009). Regulation (EC) No 450/2009 of 29 May 2009 on active and
791 intelligent materials and articles intended to come into contact with food. Official Journal
792 of European Union, 135, 3–11.
793 14. Garcia, C. V., Shin, G. H., & Kim, J. T. (2018). Metal oxide-based nanocomposites in food
794 packaging: Applications, migration, and regulations. *Trends in Food Science & Technology,*
795 *82*, 21-31. https://doi.org/10.1016/j.tifs.2018.09.021

796 15. Goudarzi, V., Shahabi-Ghahfarrokhi, I., & Babaei-Ghazvini, A. (2017/). Preparation of
797 ecofriendly UV-protective food packaging material by starch/TiO2 bio-nanocomposite:
798 Characterization. *International Journal of Biological Macromolecules, 95*, 306-313.
799 https://doi.org/https://doi.org/10.1016/j.ijbiomac.2016.11.065
800 16. Homayounpour, P., & Shariatifar, N. (2020). Development of nanochitosan-based active
801 packaging films containing free and nanoliposome caraway (Carum carvi . L) seed
802 extract. September, 553–563. https://doi.org/10.1002/fsn3.2025
803 17. Jafarzadeh, S., & Jafari, S. M. (2020). Impact of metal nanoparticles on the mechanical,
804 barrier, optical and thermal properties of biodegradable food packaging materials.
805 Critical Reviews in Food Science and Nutrition, 0(0), 1–19.
806 https://doi.org/10.1080/10408398.2020.1783200
807 18. Kaewklin, P., Siripatrawan, U., Suwanagul, A., & Lee, Y. S. (2018). Active packaging from
808 chitosan-titanium dioxide nanocomposite film for prolonging storage life of tomato fruit.
809 *International Journal of Biological Macromolecules, 112*, 523-529.
810 https://doi.org/10.1016/j.ijbiomac.2018.01.124
811 19. Khezerlou, A., Tavassoli, M., Sani, M. A., Mohammadi, K., & Ehsani, A. (2021). Application
812 of Nanotechnology to Improve the Performance of Biodegradable Biopolymer-Based
813 Packaging Materials. 1–21.
814 20. Kustiningsih, I., Ridwan, A., Abriyani, D., Syairazy, M., Kurniawan, T., & Barleany, D. R.
815 (2019). Development of Chitosan-TiO2 Nanocomposite for Packaging Film and its Ability
816 to Inactivate Staphylococcus aureus. *Oriental Journal of Chemistry, 35*(3), 1132-1137.
817 https://doi.org/10.13005/ojc/350329

21. Lan, W., He, L., & Liu, Y. (2018). Preparation and Properties of Sodium Carboxymethyl Cellulose/Sodium Alginate/Chitosan Composite Film. *Coatings, 8*(8), 291. https://www.mdpi.com/2079-6412/8/8/291

22. Lan, W., Wang, S., Zhang, Z., Liang, X., Liu, X., & Zhang, J. (2021). Development of red apple pomace extract/chitosan-based films reinforced by TiO2 nanoparticles as a multifunctional packaging material. International Journal of Biological Macromolecules, 168, 105–115. https://doi.org/10.1016/j.ijbiomac.2020.12.051

23. Li, K. J., Zhu, J. X., Guan, G. L., & Wu, H. (2019a). Preparation of chitosan-sodium alginate films through layer-by-layer assembly and ferulic acid crosslinking: Film properties, characterization, and formation mechanism. *International Journal of Biological Macromolecules, 122*, 485-492. https://doi.org/10.1016/j.ijbiomac.2018.10.188

24. Li, W., Zheng, K. W., Chen, H. J., Feng, S. R., Wang, W., & Qin, C. Q. (2019b). Influence of Nano Titanium Dioxide and Clove Oil on Chitosan-Starch Film Characteristics. *Polymers, 11*(9), Article 1418. https://doi.org/10.3390/polym11091418 Liu, Z., Du, M., Liu, H., Zhang, K., Xu, X., Liu, K., Tu, J., & Liu, Q. (2021). Chitosan films incorporating litchi peel extract and titanium dioxide nanoparticles and their application as coatings on watercored apples. *Progress in Organic Coatings, 151*, 106103. https://doi.org/https://doi.org/10.1016/j.porgcoat.2020.106103

25. Luo, Y., Lin, Z., & Guo, G. (2019). Biodegradation Assessment of Poly (Lactic Acid) Filled with Functionalized Titania Nanoparticles (PLA/TiO 2) under Compost Conditions. Nanoscale Research Letters, 14. https://doi.org/10.1186/s11671-019-2891-4

839 26. Mulla, M. Z., Rahman, M. R. T., Marcos, B., Tiwari, B., & Pathania, S. (2021). Poly Lactic
840 Acid (PLA) Nanocomposites: Effect of Inorganic Nanoparticles Reinforcement on Its
841 Performance and Food Packaging Applications. *Molecules, 26*(7), Article 1967.
842 https://doi.org/10.3390/molecules26071967
843 27. Othman, S. H., Othman, N. F. L., Shapi'i, R. A., Ariffin, S. H., & Yunos, K. F. (2021). Corn
844 Starch / Chitosan Nanoparticles / Thymol Packaging Applications. Polymers, 13(390).
845 28. Pires, J. R. A., Souza, V. G. L., Fuciños, P., Pastrana, L., & Fernando, A. L. (2022).
846 Methodologies to Assess the Biodegradability of Bio-Based Polymers—Current
847 Knowledge and Existing Gaps. *Polymers*, *14*(7), 1359.
848 https://doi.org/10.3390/polym14071359
849 29. Phothisarattana, D., & Harnkarnsujarit, N. (2022). Migration , aggregations and thermal
850 degradation behaviors of TiO 2 and ZnO incorporated PBAT / TPS nanocomposite blown
851 films. Food Packaging and Shelf Life, 33(January), 100901.
852 https://doi.org/10.1016/j.fpsl.2022.100901
853 30. Riahi, Z., Priyadarshi, R., Rhim, J. W., & Bagheri, R. (2021). Gelatin-based functional films
854 integrated with grapefruit seed extract and TiO2 for active food packaging applications.
855 Food Hydrocolloids, 112(September 2020), 106314.
856 https://doi.org/10.1016/j.foodhyd.2020.106314
857 31. Rodriguez-Uribe, A., Wang, T., Pal, A. K., Wu, F., Mohanty, A. K., & Misra, M. (2021).
858 Injection moldable hybrid sustainable composites of BioPBS and PHBV reinforced with
859 talc and starch as potential alternatives to single-use plastic packaging. Composites Part
860 C: Open Access, 6, 100201. https://doi.org/10.1016/j.jcomc.2021.100201

32. Ruan, C., Zhang, Y., Wang, J., Sun, Y., Gao, X., Xiong, G., & Liang, J. (2019). Preparation and antioxidant activity of sodium alginate and carboxymethyl cellulose edible films with epigallocatechin gallate. International Journal of Biological Macromolecules, 134, 1038–1044. https://doi.org/10.1016/j.ijbiomac.2019.05.143

33. Salama, H. E., & Abdel Aziz, M. S. (2020). Optimized carboxymethyl cellulose and guanidinylated chitosan enriched with titanium oxide nanoparticles of improved UV-barrier properties for the active packaging of green bell pepper. International Journal of Biological Macromolecules, 165, 1187–1197. https://doi.org/10.1016/j.ijbiomac.2020.09.254

34. Salama, H. E., Abdel Aziz, M. S., & Sabaa, M. W. (2018). Novel biodegradable and antibacterial edible films based on alginate and chitosan biguanidine hydrochloride. International Journal of Biological Macromolecules, 116, 443-450. https://doi.org/https://doi.org/10.1016/j.ijbiomac.2018.04.183

35. Şen, F., Uzunsoy, İ., Baştürk, E., & Kahraman, M. V. (2017). Antimicrobial agent-free hybrid cationic starch/sodium alginate polyelectrolyte films for food packaging materials. Carbohydrate Polymers, 170, 264–270. https://doi.org/10.1016/j.carbpol.2017.04.079

36. Sani, M. A., Azizi-lalabadi, M., Tavassoli, M., Mohammadi, K., & Mcclements, D. J. (2021). Recent Advances in the Development of Smart and Active Biodegradable Packaging Materials. 1–34.

37. Sani, M., Maleki, M., Eghbaljoo-Gharehgheshlaghi, H., Khezerlou, A., Mohammadian, E., Liu, Q., & Jafari, S. M. (2022). Titanium dioxide nanoparticles as multifunctional surface-active materials for smart/active nanocomposite packaging films. Advances in Colloid and

883 Interface Science, 300(December 2021), 102593.
884 https://doi.org/10.1016/j.cis.2021.102593
885 38. Shahbazi, Y., & Shavisi, N. (2020). Application of active Kurdi gum and Farsi gum-based
886 coatings in banana fruits. Journal of Food Science and Technology, 57(11), 4236–4246.
887 https://doi.org/10.1007/s13197-020-04462-x
888 39. Shahbazi, Y., Shavisi, N., & Karami, N. (2021). Development of edible bioactive coating
889 based on mucilages for increasing the shelf life of strawberries. Journal of Food
890 Measurement and Characterization, 15(1), 394–405. https://doi.org/10.1007/s11694-
891 020-00638-3
892 40. Shanmugam, B. K., Rangaraj, S., Subramani, K., Srinivasan, S., Aicher, W. K., &
893 Venkatachalam, R. (2020). Biomimetic TiO2-chitosan/sodium alginate blended
894 nanocomposite scaffolds for tissue engineering applications. *Materials Science &*
895 *Engineering C-Materials for Biological Applications, 110*, Article 110710.
896 https://doi.org/10.1016/j.msec.2020.110710
897 41. Shehata, S. A., Abdelrahman, S. Z., Megahed, M. M. A., Abdeldaym, E. A., El-Mogy, M. M.,
898 & Abdelgawad, K. F. (2021). Extending Shelf Life and Maintaining Quality of Tomato Fruit
899 by Calcium Chloride, Hydrogen Peroxide, Chitosan, and Ozonated Water. *Horticulturae,*
900 *7*(9), 309. https://www.mdpi.com/2311-7524/7/9/309
901 42. Siripatrawan, U., & Kaewklin, P. (2018). Fabrication and characterization of chitosan-
902 titanium dioxide nanocomposite film as ethylene scavenging and antimicrobial active
903 food packaging. *Food Hydrocolloids, 84*, 125-134.
904 https://doi.org/10.1016/j.foodhyd.2018.04.049

905 43. Sooch, B. S., & Mann, M. K. (2021). Nanoreinforced biodegradable gelatin based active
906 food packaging film for the enhancement of shelf life of tomatoes (Solanum lycopersicum
907 L.). *Food Control, 130*, 108322.
908 https://doi.org/https://doi.org/10.1016/j.foodcont.2021.108322
909 44. Sun, R., Zhu, J., Wu, H., Wang, S., Li, W., & Sun, Q. (2021). Modulating layer-by-layer
910 assembled sodium alginate-chitosan film properties through incorporation of cellulose
911 nanocrystals with different surface charge densities. *International Journal of Biological*
912 *Macromolecules, 180*, 510-522.
913 https://doi.org/https://doi.org/10.1016/j.ijbiomac.2021.03.092
914 45. Tang, S., Wang, Z., Li, P., Li, W., Li, C., Wang, Y., & Chu, P. K. (2018). Degradable and
915 photocatalytic antibacterial Au-TiO2/sodium alginate nanocomposite films for active food
916 packaging. Nanomaterials, 8(11). https://doi.org/10.3390/nano8110930
917 46. Wen, J. W., Huang, S. T., Sun, Y., Chen, Z. J., Wang, Y. X., Li, H. B., & Liu, X. H. (2018).
918 Titanium Dioxide Nanotube-Based Oxygen Indicator for Modified Atmosphere Packaging:
919 Efficiency and Accuracy. *Materials, 11*(12), Article 2410.
920 https://doi.org/10.3390/ma11122410
921 47. Xiong, J., Sheng, C., Wang, Q., & Guo, W. (2019). Toughened and water-resistant
922 starch/TiO2 bio-nanocomposites as an environment-friendly food packaging material.
923 *Materials Research Express*, *6*(5). https://doi.org/10.1088/2053-1591/ab058b
924 48. Yu, Z., Wang, W., Sun, L., Kong, F., Lin, M., & Mustapha, A. (2020). Preparation of
925 cellulose nanofibril/titanium dioxide nanoparticle nanocomposites as fillers for PVA-
926 based packaging and investigation into their intestinal toxicity. *International Journal of*

927 *Biological Macromolecules, 156*, 1174-1182.
928 https://doi.org/https://doi.org/10.1016/j.ijbiomac.2019.11.153
929 49. Zamanian, M., Sadrnia, H., Khojastehpour, M., Hosseini, F., Kruczek, B., & Thibault, J.
930 (2021). Barrier Properties of PVA/TiO2/MMT Mixed-Matrix Membranes for Food
931 Packaging. Journal of Polymers and the Environment, 29(5), 1396–1411.
932 https://doi.org/10.1007/s10924-020-01965-8
933 50. Zhang, W. L., & Rhim, J. W. (2022). Titanium dioxide (TiO2) for the manufacture of
934 multifunctional active food packaging films. *Food Packaging and Shelf Life, 31*, Article
935 100806. https://doi.org/10.1016/j.fpsl.2021.100806
936 51. Zhang, X., Liu, Y., Yong, H., Qin, Y., Liu, J., & Liu, J. (2019). Development of multifunctional
937 food packaging films based on chitosan, TiO2 nanoparticles and anthocyanin-rich black
938 plum peel extract. *Food Hydrocolloids, 94*, 80-92.
939 https://doi.org/https://doi.org/10.1016/j.foodhyd.2019.03.009
940 52. Zhang, X., Xiao, G., Wang, Y., Zhao, Y., Su, H., & Tan, T. (2017). Preparation of chitosan-
941 TiO2 composite film with efficient antimicrobial activities under visible light for food
942 packaging applications. Carbohydrate Polymers, 169, 101–107.
943 https://doi.org/10.1016/j.carbpol.2017.03.073
944
945
946